Daniela Reichstam BSc.

Application of block theory for the rapid identification of hazardous blocks in a natural rock slope

MASTER'S THESIS

to achieve the university degree of

Master of Science

Master's degree programme: Earth Sciences

submitted to

Graz University of Technology

Supervisor

Ao.Univ.-Prof. Dr. Qian Liu

Instiiute of Applied Geosciences

Graz, March 2017

AFFIDAVIT

I declare that I have authored this thesis independently, that I have not used other than the declared sources/resources, and that I have explicitly indicated all material which has been quoted either literally or by content from the sources used. The text document uploaded to TUGRAZonline is identical to the present master's thesis.

_____	_____
Date	Signature

DANKSAGUNG

An dieser Stelle möchte ich allen Danken, die mich bei der Verfassung dieser Masterarbeit motiviert und unterstützt haben. Aber auch all jenen, die mich über die letzten Jahre während meines Studiums begleitet und inspiriert haben.

Ein besonderer Dank gilt an dieser Stelle Ao.Univ.-Prof. Dr. Qian Liu als dem Betreuer dieser Arbeit. Nur durch seine Ideen und die fachliche Unterstützung bin ich am heutigen Punkt angelangt. Sein starker Glaube an mich und mein Können waren mir immer eine Stütze. Danke nochmals für die Zeit und das Engagement mit dem er mich betreut hat.

Ebenso möchte ich Mag. Dr.tech. Wolfgang Jaritz danken, der mir die Möglichkeit gab bereits während der Erstellung dieser Masterarbeit in die Arbeitswelt der Geologen einzutauchen. Dank gilt auch dem Verständnis und der Anerkennung die er mir immer entgegen bringt.

Ein großer Dank gilt meinem Freund David der sich um alle EDV-technischen Belange kümmerte. Ohne ihn wäre diese Masterarbeit wohl mit Hammer und Meißel erstellt worden. Danke auch für den guten Zuspruch und die Unterstützung über die letzten Jahre und insbesondere während der letzten Zeit.

Zum Abschluss möchte ich meinen Eltern danken, die mir erst ermöglicht haben, dieses Studium zu absolvieren. Danke für die jahrelange Unterstützung und das Vertrauen in mich.

KURZFASSUNG

In dieser Masterarbeit wurde die Block Theorie an natürlichen Felsböschungen zur Identifizierung von gefährlichen Blöcken angewandt.

Im Jahre 1985 wurde die Block Theorie von Goodman und Shi eingeführt und seitdem an unterschiedlichen Tunnelprojekten getestet. Ihre Anwendung an natürlichen Felsböschungen ist jedoch neuartig. Nach einer kurzen Einführung in die Block Theorie wird auf die verschiedenen Arten der Datenerfassung eingegangen. Anschließend wird die Methodik zur Anwendung der Block Theorie auf natürliche Felsböschungen beschrieben. Im ersten Schritt werden die Blockformen im Feld identifiziert, danach rekonstruiert und dargestellt und zuletzt hinsichtlich ihrer Stabilitätsparameter beurteilt. Für die Analyse werden lediglich die Trennflächenparameter Orientierung, Abstand und Reibungswinkel benötigt. In der abschließenden Feldstudie wurden versagte Blöcke an zwei verschiedenen Standorten, einer im Kristallin und einer im Karbonat, analysiert.

Die Ergebnisse dieser Masterarbeit belegen, dass die Block Theorie an natürlichen Felsböschungen angewandt werden kann und die schnelle Identifizierung von gefährlichen Blöcken erlaubt.

ABSTRACT

In this master thesis block theory was applied on natural rock slopes to identify hazardous blocks. Therefor block moulds were used to show its applicability.

Block theory was first introduced by Goodman and Shi in 1985. Since then it has successfully been used on different excavation sites. On the other hand the application on natural rock slopes is novel. After a short introduction into block theory the different types of data acquisition are described. The methodology for the application of block theory on natural rock slopes is described afterwards. First step is the identification of block moulds, second their reconstruction and visualisation and third the analysis regarding their stability. The only needed input parameters for the analysis are the joint orientation, spacing and friction angle. In the subsequent field study block moulds on two different sites, one in carbonate and one in crystalline, were analysed.

The results of this master thesis proof that the application of block theory on natural slopes is not only possible but also allows a rapid identification of hazardous blocks.

1. INTRODUCTION

The general idea of this master thesis is the application of block theory on natural rock slopes. It should be determined if block theory can be used for the rapid identification of potential hazardous blocks based on the in-situ joint parameters orientation, spacing and friction angle.

In the past different kinds of rock mass classification had been used in engineering geology. But putting a highly complex system as a discontinuous rock mass into simplified categories may lead to wrong conclusions concerning rock behaviour. Riedmüller and Schubert (1999) listed the major shortcomings of rock mass classification:

- Classification parameters are not well defined and sufficient to select adequate design parameters and tunnel support.
- Complex properties of a rock mass cannot sufficiently be described by a single number.
- The same rating can be achieved by various combinations of classification parameters.

After Goodman and Shi (1985) introduced block theory in 1985 it has been applied on different types of rock excavations instead of and/or complementary to rock mass classification. But studies on actual excavation sites (Hatzor, 1993) have shown that the theoretical approaches of block theory did not provide a real natural hazardous block necessarily. Although block theory may establish a theoretical hazardous block it cannot be found in nature at the excavation site. A new method called *"The critical key block concept"* was established by Goodman and Hatzor (1990) to detect actual hazardous blocks. A critical key block is found by applying block theory and is determined by the relative block failure likelihood distribution P(B). This block failure likelihood is a function of the joint set parameters orientation, relative spacing and friction angle. Using block moulds, which originate from already failed blocks, the *"critical key block concept"* (Goodman and Hatzor, 1990) had been tested and was thereby confirmed on various excavation sites (Hatzor and Goodman, 1993, 1995; Hatzor, 1993).

So far block theory and the critical key block concept have been used on different excavation sites. The application of block theory on natural rock slopes, as shown in this thesis, is novel.

The application of block theory should be as simple and on the other hand as precise as possible. Therefore the data acquisition is the crucial point. Extensive data collection would lead to an unnecessary time loss whereby too simple methods may not provide the necessary data. On that account it will be part of this thesis to obtain which data is necessary, how it can be gained and which advantages the different methods of data collection offer.

Finally this new approach is tested on different rock slope sites using block moulds. It should be determined whether using block theory on natural rock slopes is reasonable and useful for actual applications.

2.   AN INTRODUCTION TO BLOCK THEORY

2.1.   GENERAL

In the following chapters a short introduction to block theory is given. Numerous papers were written about the application of block theory (Goodman and Hatzor, 1990; Hatzor and Goodman, 1993, 1995; Hatzor, 1993). If not mentioned otherwise the content of this chapter was taken from Goodman and Shi (1985).

2.2.   AN INTRODUCTION TO BLOCK THEORY AND HALF-SPACE-CODES

With block theory the analysis of possible instable free faces can be done:

- It identifies removable blocks, formed by discontinuities and free surfaces.
- It determines the block morphology: its volume, area of faces, position of vertexes and position of faces and edges.
- A kinematic and static equilibrium analysis of key blocks under self-weight, applied forces and the given friction angle is done.

The only necessary parameters are the orientation, spacing and friction angle of the governing discontinuities and the free face. These data can be gained in numerous different ways, with some examples in chapter 3. By plotting the poles (normals) of each recorded discontinuity (regardless the genetic evolution) as stereographic projections the governing discontinuities can be identified.

Since rock masses are not a continuous medium several assumptions have to be made to apply block theory:

- Discontinuity surfaces are planar.
- Discontinuity surfaces have an infinite extend.
- Blocks are rigid and not subject to distortion or deformation.
- Free face and discontinuity parameters are assumed to be determined.

The so-called half-space-codes are a main part of block theory. A Joint always divides the three-dimensional space into two parts, the two half-spaces. The upper half-space, which is on top of the joint has the half-space-code 0 (sometimes referred to as U). Reverse the lower half-space under the joint has the half-space-code 1 (sometimes referred to as L). They are used to describe the three-dimensional position of a block relating to the relevant joint sets. Since a block is always defined by at least four surfaces (= planes), it is defined by the half-space of each plane it is part of.

In lower hemisphere projection the upper half-space (0 or U) is represented by the area outside the great circle and the lower half-space (1 or L) is represented by the area inside the great circle. In Figure 1 the planes 1 (red), 2 (blue), 3 (green) and one free plane (dashed) are visualised. The block with the half-space-code 110 for example is formed below the planes 1 (red) and 2 (blue) and above plane 3 (green).
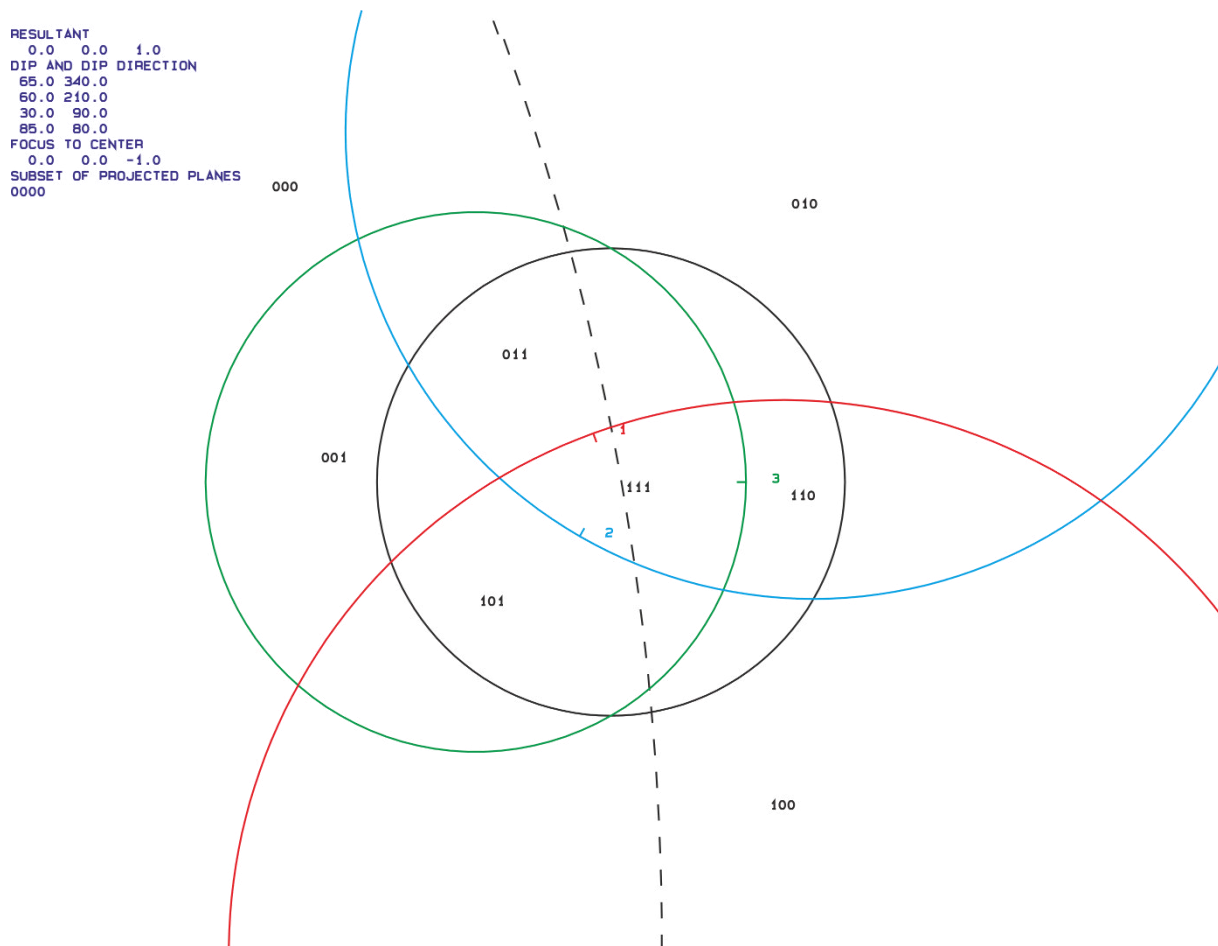
Figure 1: Example of half-space-codes (lower hemisphere projection), black circle: reference circle, red: plane 1, blue: plane 2, green: plane 3.

For the further discussion some definitions have to be made:

- To simplify the descriptions the word joint is used, no matter which origin or genetic evolution the discontinuity has.
- A joint combination **JC** is the point where two or more joints of different joint sets intersect in space. It is represented in stereographic projection as a point.
- A joint pyramid **JP** is the area in space where all joints of a block meet if they are shifted to a common origin. It is represented in stereographic projection as the area bounded by joint plane great circles. The JP half-space-code gives information about whether a block is built above or under a joint. In lower hemisphere projection 0 means upper half-space (inside the great circle) and 1 means lower half-space (outside the great circle).
- The excavation pyramid **EP** is the area behind the excavation (= free) surface.
- The space pyramid **SP** is the area in front of the excavation (= free) surface.
- A block pyramid **BP** is the intersection of the JP with the EP.

2.3. BLOCK TYPES

There are different types of blocks, which were stated by Goodman and Shi (1985) and are listed in Table 1. The different block types are visualised in Figure 2.

Table 1: Block types stated by Goodman and Shi (1985).

BLOCK TYPES				
INFINITE	FINITE			
V	Non removable	Removable		
-	IV tapered	III stable even without sufficient friction	II stable with sufficient friction	I unstable without support
-	-	-	POTENTIAL KEYBLOCK	KEYBLOCK

Removable blocks
I   Keyblock
II   Potential keyblock
III   Stable block

Non removable block
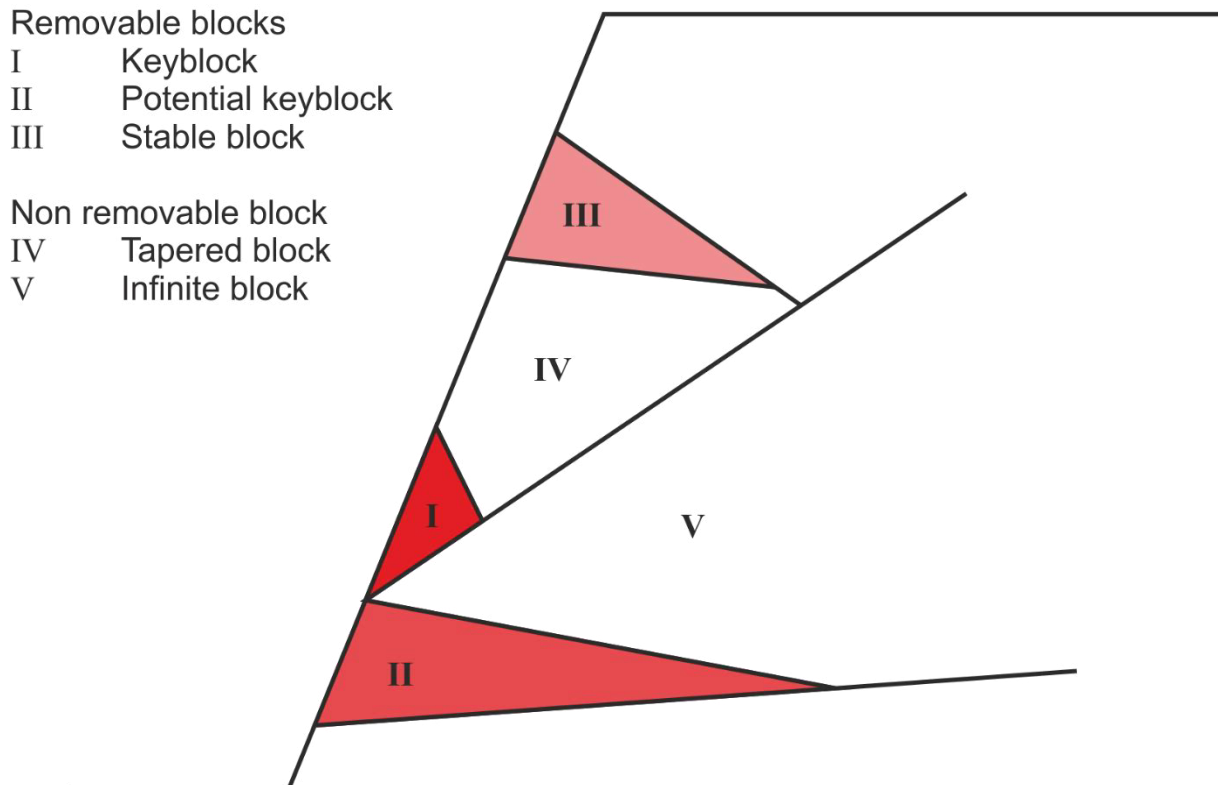IV   Tapered block
V   Infinite block

Figure 2: Different block types after Goodman and Shi (1985). Visualisation after Liu (2014).

Shi´s Theorem of finiteness (Goodman and Shi, 1985) states the following:

> "A convex block is finite if its block pyramid is empty. Conversely, a convex block is infinite if its block pyramid is not empty."

$$JP \cap EP = 0$$

$$BP = JP \cap EP = 0$$

$$SP = \sim EP$$

$$JP \subset SP$$

This means a JP has to be entirely contained in the SP to form a finite block, and only finite blocks may form a removable block.

Shi´s Theorem on removability (Goodman and Shi, 1985) states the following:

> "A convex block is removable if its block pyramid is empty and its joint pyramid is not empty. A convex block is not removable (tapered) if its block pyramid is empty and its joint pyramid is empty."

By applying this rule only removable blocks are left for further analysis.

With n non parallel joints 2^n JP can be created. The number of not empty JPs is:

$$N_R = n^2 - n + 2$$

Where:

N_R .... *Number of not empty JPs*

n .... *Number of joints*

Since the number of JPs intersecting the EP is 2n the number of JP ∩ EP = 0 is:

$$N_r = n^2 - n + 2 - 2n = n^2 - 3n + 2$$

Where:

N_r .... *Number of finite BPs*

n .... *Number of joints*

N_r is the amount of BPs which are finite.

The number of removable finite blocks is the result of the combination of JPs with EP which have no intersection with the EP. It is defined as:

$$N_{PKB} = \frac{N_r}{2} = \frac{n^2 - 3n + 2}{2}$$

Where:

N_{PKB} .... *Number of removable finite blocks*

N_r .... *Number of finite BPs*

n .... *Number of joints*

This is the number of BPs which are classified as removable. For the following analysis of block shape, kinematic and limit equilibrium only the removable blocks are considered.

2.4. BLOCK FAILURE PROBABILITY

2.4.1. GENERAL

To improve the reliability of block theory the probability of block failure likelihood was introduced with the "*critical keyblock concept*" (Goodman and Hatzor, 1990). This new approach has been approved and extended in numerous continuative researches (Hatzor and Goodman, 1993, 1995; Hatzor, 1993). Six main steps were defined and used by Goodman and Hatzor (1990) to determine the block failure likelihood. The content of the following chapters 2.4.2 to 2.4.7 was, if not indicated otherwise, taken from Goodman and Hatzor (1990).

2.4.2. FINDING GOVERNING JOINT SETS

After a detailed mapping or data acquisition a statistical analysis of joint set poles plotted in stereographical projection has to be done to find the governing joint sets. They are the product of the tectonic history and the geological setting of a site. Therefore they can be seen as the representative structural input for further analysis.

If two or more joint sets have the same orientation only one is used for the following analysis.

2.4.3. FINDING JOINT COMBINATIONS JC

Using the before defined governing joint sets the number of possible joint combinations is computed. This number represents the potential number of joint combinations, excluding combinations with repeated joint sets. A block is defined by at least four planes. There are different ways to comprise a block from a combination of joint and free planes (Figure 3). Since at least one joint plane is needed to form a block the minimum value for the number of joint sets which comprise the JP boundaries k is 1. The maximum value for k is n. Observations have shown that the most likely value is 3.
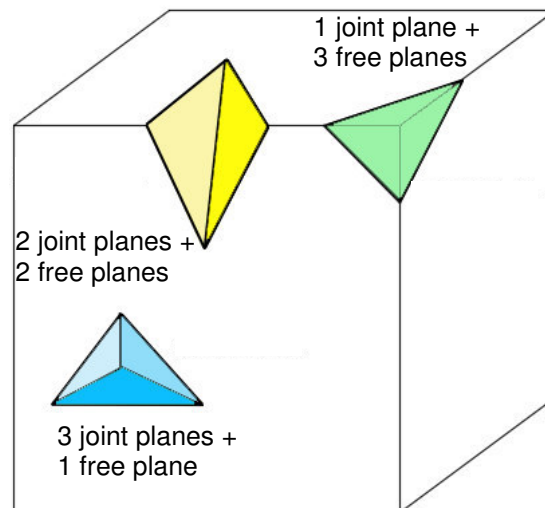
Figure 3: Different combinations of block building planes. At least four planes are needed to form a block. Image taken from and modified after Molterer (2015) after Kieffer (2012).

$$N_{JC} = \frac{n!}{k! \cdot (n-k)!}$$

Where:

N_{jc} .... *Number of joint combinations [-]*

n .... *Number of governing joint sets [-]*

k .... *Number of joint sets which comprise the JP boundaries [-]*

2.4.4. FINDING REMOVABLE JOINT PYRAMIDS JP

Not all of the JC build a removable JP. Therefore block theory has to be applied to find the removable JP. A removable JP has no intersection with the excavation pyramid (EP), as stated by Shi´s Theorem (Goodman and Shi, 1985). Per definition a JP is safe if the intersection of two joint sets is included in the plane of the free face. All JCs including this two joint sets are regarded to be unremovable.

$$N_{rb} = \frac{n!\,(k^2 - 3k + 2)}{k!\,(n-k)!\,2}$$

Where:

N_{rb} .... *Number of removable blocks [-]*

N .... *Number of governing joint sets [-]*

k .... *Number of joint sets which comprise the JP boundaries [-]*

2.4.5. JOINT COMBINATION PROBABILITY P[JC]

It is obvious that more closely spaced joint sets are more likely to form joint combinations. For a numerical investigation a negative exponential distribution of the discontinuity spacing is assumed.

$$f(x) = \lambda e^{-\lambda x}$$

Where:

$f(x)$ .... *Frequency of discontinuity spacing x [1/m]*

λ .... *Number of discontinuities per unit length [1/m]*

x .... *Spacing [m]*

To find the spacing of the governing joint sets a scanline analysis can be used. The real frequency of discontinuities is a function of the measured frequency and the angle between joint set and scanline.

$$\lambda = \lambda_\theta / cos\theta$$

Where:

λ .... *True frequency of discontinuities [1/m]*

λ_θ .... *Observed frequency of discontinuities [1/m]*

θ .... *Angle between scanline and joint [°]*

The probability to find a specific number of joints is a Poisson process.

$$P[N(I) = k] = e^{-\lambda x} \frac{\lambda x^k}{k!}$$

Where:

P[N(I) = k] … Probability of joint sets N over a fixed interval I [-]

    x ……. Length of Intervall I [m]

    λ ……. True frequency of discontinuities [1/m]

    k ……. Number of joint sets which comprise the JP boundaries [-]

The probability to find more than zero intersection of a given joint set I over a length x.

$$P[N(I)\_i > 0] = 1 - P[N(I)\_i = 0] = 1 - e^{-\lambda_i x}$$

Where:

P[N(I)_i>0] … Probability of more than zero intersection of joint set I [-]

    x ……. Length of intervall I [m]

    λ_i ……. True frequency of joint set I [1/m]

Combining this formula for all joint sets the probability for a joint combination can be obtained.

$$P(JC) = [1 - e^{-\lambda_i x}] \cdot [1 - e^{-\lambda_j x}] \cdot [1 - e^{-\lambda_k x}]$$

Where:

  P(JC) ……. Joint combination probability [-]

    x ……. Length of intervall I [m]

$\lambda_i, \lambda_j, \lambda_k$ ……. True frequency of joint set i, j, k [1/m]

Or with the formula by (Hatzor, 1993).

$$P(JC) = (\lambda_i \lambda_j \lambda_k)|n_i \cdot n_j \times n_k|$$

Where:

$P(JC)$ .... *Joint combination probability [-]*

$\lambda_i, \lambda_j, \lambda_k$ .... *Joint set true frequency [1/m]*

n_i, n_j, n_k .... *Joint set normal [-]*

2.4.6. DEGREE OF HAZARD FOR REMOVABLE JOINT PYRAMIDS K

The degree of hazard for a removable JP is defined by the area of its spherical triangle in stereographic projection (Mauldon, 1994). It is also known as shape parameter (Hatzor, 1993).

$$K = \frac{area\ of\ JP\ spherical\ triangle}{area\ of\ the\ sphere} = \frac{[A + B + C - \pi] \cdot R^2}{4 \cdot \pi \cdot R^2}$$

Where:

K .... *Degree of hazard for a removable JP*

A, B, C .... *Angles between the JP boundaries [rad]*

R .... *Radius of the stereographic projection plane [m]*

An easy estimation if a JP is hazardous can be seen by its apex. A large apex distance is less dangerous than a small one.

On openings with parallel free faces cousin-JPs are removable on the cousin free face. A cousin is built by changing the half space codes to the opposite ones. When working on slopes cousin free faces and JPs are not a topic.

2.4.7.   OVERALL BLOCK FAILURE PROBABILITY P[B] (GOODMAN AND HATZOR, 1990)

The actual likelihood of a JP to fail in combination with the free face is computed by using the degree of hazard K and its JC probability.

$$P[B] = K \cdot P[JC]$$

Where:

P[B] .... *Overall block failure probability*

K .... *Degree of hazard for a removable JP*

P[JC] .... *Joint combination probability*

2.4.8.   IMPROVED BLOCK FAILURE PROBABILITY P(B) WITH AN ADDITIONAL PARAMETER F (HATZOR, 1993)

Hatzor (1993) introduced another factor into the analysis of block failure likelihood. The block instability parameter F is a product of the net sliding force and the active resultant force (Table 2).

$$F = 2^{\left(\frac{F^*}{R}\right) - 1}$$

Where:

F .... *Block instability parameter [-]*

F* .... *Net sliding force [N]*

R .... *Active resultant force [N]*

For falling:

$$F^* = |r|$$

For single face sliding:

$$F^* = |\hat{n}_i \times r| - |\hat{n}_i \cdot r| \tan\phi_i$$

For double face sliding:

$$F^* = \frac{1}{|\hat{n}_i \times \hat{n}_j|^2}\{|r \cdot (\hat{n}_i \times \hat{n}_j)||\hat{n}_i \times \hat{n}_j| - |(r \times \hat{n}_j) \cdot (\hat{n}_i \times \hat{n}_j)|tan\phi_i - |(r \times \hat{n}_i) \cdot (\hat{n}_i \times \hat{n}_j)|tan\phi_j\}$$

Where:

F^* .... *Net sliding force [N]*

R .... *Active resultant [N]*

n_i, n_j .... *Joint normal of joint i and j*

ϕ_i, ϕ_j .... *Joint angle of joint i and j [rad]*

Table 2: Relationship between normalized sliding force, failure mode and instability parameter F (after Hatzor, 1993).

F^* / R	FAILURE MODE	INSTABILITY PARAMETER F
1.0	Falling	F = 1
0 – 1.0	Sliding	0.5 < F < 1.0
0	Limit equilibrium	F = 0.5
< 0	Safe	0 < F < 0.5
∞	No mode	F = 0

The overall block failure probability by Hatzor (1993) is computed similar to the block failure probability by Goodman and Hatzor (1990). Only the instability parameter F is added.

$$P(B) = P(JC) \cdot K \cdot F$$

Where:

$P(B)$ .... *Block failure probability [-]*

$P(JC)$ .... *Joint combination probability [-]*

K .... *Shape parameter, degree of hazard for a removable JP [-]*

F .... *Block instability parameter [-]*

2.4.9. FIELD STUDIES OF BLOCK FAILURE PROBABILITY

Goodman and Hatzor (1990) applied the before described steps (chapter 2.4.2 to 2.4.7) on block moulds on the sidewalls of tunnels.

The number of discontinuities building a JP k = 3 is valid since only 2 of 35 showed k = 4. Sliding along pre-existing planes is the main failure mode. Only one failure occurred along a blasting induced discontinuity. Nearly all blocks which have failed were predicted by block theory. Therefore block theory can be accepted as a good tool to predict failing blocks. The few blocks which were not predicted could have been foreseen if only one additional joint set had been added to the analysis.

The probability prediction, as described in chapter 2.4.2 to 2.4.7, is reasonable since 15 of the 23 failed blocks were formed by one JP with the highest failure probability P[B]. For a fast estimation of the failure probability the joint set frequency and the angles between the joint planes can be used. A high joint set frequency and large angles between the planes indicate a higher failure likelihood.

One last indication for a higher failure likelihood is a low angle between the free face and the discontinuities or intersections of discontinuities.

A correlation between block failure probability P(B), natural block moulds and the respective parameters was done by Hatzor (1993).

The correlation between joint combination probability P(JC) and the block moulds exhibited a positive linear regression with a correlation coefficient R of 0.82 for the realistic least square method. This means the higher the P(JC) the higher the percentage of block moulds found at the site.

The instability parameter F of all found moulds had a value > 0.45, which implies that the assumption of F = 0.5 as limit equilibrium can be seen as true. Block moulds with F < 0.5 could be caused by excavation activity.

The shape parameter K has a weaker correlation since it is just a scaling parameter of how hazardous a block is. The correlation in hard crystalline rock was better than in the sedimentary carbonate sequence. This could be caused by the simple fact that the before made assumptions are better fulfilled in hard rock masses. Whereas in sedimentary structures the full shape of the calculated blocks is never reached since the discontinuities are not infinite.

A correlation between the modified P(B)` and the block mould amount showed a good correlation of 0.72 and a slope of 1.02.

$$P(B)` = P(JC) \cdot F$$

P(B)` .... Modified block failure likelihood

P(JC) .... Joint combination probability

F .... Instability parameter

Therefore the shape parameter could be excluded or modified for a better fit of the overall block failure probability P(B).

2.5. DISCUSSION

Block theory had been proven to be a suitable tool for the identification of hazardous blocks in artificial excavation sites using the block failure likelihood. But still some issues have to be taken into account.

Block theory is still a theoretical approach based on unified parameters like joint set orientation, spacing and friction angle. Having a three-dimensional discontinuous rock mass this simplification has to be kept in mind. On the other hand these parameters can be gained fairly easy during any stage of excavation and therefore the analysis with block theory can be adapted to the newly gained data.

Furthermore block theory is based on four critical assumptions (Goodman and Shi, 1985), which are:

- Discontinuity surfaces are planar.
- Discontinuity surfaces have an infinite extend.
- Blocks are rigid and not subject to distortion or deformation.
- Excavation face and discontinuity parameters are assumed to be determined.

Rock masses are a product of development over thousands of years, exposed to various influencing factors. The assumptions stated above cannot be regarded as correct infinitely in all three dimensions.

There are further methods for the identification of hazardous blocks such as the use of so-called trace maps. The trace map of a site contains all visible joint traces of a slope at one specific moment. Using block theory a potential keyblock can be identified and visualised on the tracemap and later found on the natural slope. In Figure 4 a classic trace map with three different joint planes is shown. As an example two potential keyblocks with the half-space-code 101 are highlighted in grey.
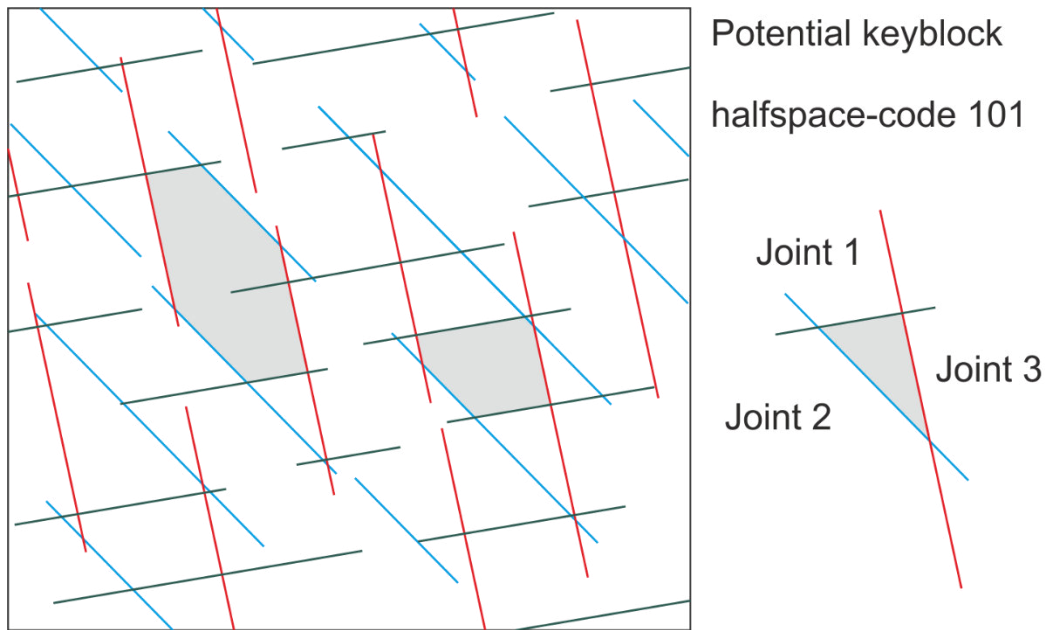
Figure 4: Example of a trace map of a rock slope with three different joint sets.

The biggest limitation by using trace maps is the two-dimensional data. A trace map only shows what is visible at a rock slope at a given time. Three-dimensional parameters like persistence or termination cannot be taken into account.

3. DATA ACQUISITION

3.1. GENERAL

The input parameters for block theory are the joint set orientation, spacing and friction angle. These parameters are usually gained by finding the governing joints of a site and averaging the collected data for each joint set. Therefore the data acquisition is a crucial point.

An extensive and accurate type of data collection would bring a more precise mean value but is most likely more time and cost intensive. On the other hand a faster, easier and probably cheaper method could presumably lead to less accurate results.

Furthermore different types of methods can yield different types of data. The measurement with a geological compass will only provide two-dimensional data based on statistical joint set evaluation. Terrestrial laser scanning (LiDAR) in contrast provides three-dimensional georeferenced data of block moulds, which can be analysed related to a specified location.

Therefore different types of data acquisition are described in the following chapters.

3.2. TERRESTRIAL LASER SCANNING (LIDAR)

3.2.1. GENERAL

Terrestrial laser scanning, or **Li**ght **D**etecting **A**nd **R**anging (LiDAR), has been in focus over the last years for geological data acquisition. The enhancement of technology and equipment have led to a wide range of application. Therefore various studies had been done to point out the assets and drawbacks as well as the numerous ways of application.

Buckley et al. (2008) provided a good abstract about data acquisition, processing and accuracy considerations. Different types of application have been shown in Fekete et al. (2010), Liu and Kieffer (2011, 2012), Liu (2014, 2016) and Liu and Kaufmann (2015). These studies are summarized below to give an overview about the application of LiDAR.

3.2.2. DATA ACQUISITION AND POST-PROCESSING

There are two different types of scanners which are commonly used for geological purpose, pulse ranging and continuous wave (cw) ranging (Thiel and Wehr, 2004). Pulse ranging scanners emit a very short laser pulse with a high energy peak level and measure the return time of the laser pulse to the receiver. CW-scanners also emit a laser beam, but in contrast to pulse ranging scanners, a continuous beam with modulated intensity is send out.

Independent of the ranging type the result of a laser scan is a three-dimensional point cloud, each point defined by X, Y, Z coordinates. Before carrying out a LiDAR survey the work flow has to be set, adopted to the required data and the aim of the study.

The resolution has to be synchronised to the scale of the geological unit which is going to be measured. A higher resolution always leads to a longer scanning time and a higher amount of data in the point cloud, which does not necessary pays off in a gain of more information.

The scanning position determines the possible collected data. A clear line of sight as well as the geometrical arrangement to the site and the atmospheric conditions are influencing factors. Although high humidity as well as vegetation do not block the laser beam completely, the quality of the result can decrease rapidly and/or more post-processing is necessary. The positon should be as far as possible orthogonal to and on the same height as the target. Otherwise so-called "shadows" (occlusions) lower the quality of the collected data. Therefore different scan positions should be chosen to guarantee a good coverage and a high quality of the collected data.

By using referenced points or for example RTK-GPS to determine the absolute positon of the scanner the three-dimensional point clouds of different scan positons can be positioned relatively and absolutely in space.

In addition to the three-dimensional point cloud a true-colour image of the site can be collected to supplement the collected data. Usually the camera is mounted directly on the scanner.

The first part of post-processing is the scan registration by which all scans of different scan positions are referenced relatively to each other. Otherwise only single scans can be viewed and the big advantage of large-area coverage is lost. Two different approaches are possible for relative positioning, either by mathematical algorithms or by referenced tie points. In addition the three-dimensional point cloud can be referenced to a global coordinate system. This allows for example the correlation of different sites over large distances. For absolute positioning it is common to register the coordinates of the scanner at each scan positon by a GPS antenna. But the absolute positon of the scanner does not provide the orientation of the scanned site. Therefore at least three overlapping scan positions are needed to specify the orientation of the point cloud.

Although the raw point cloud allows an interpretation of the scan data to some extend and offers the highest accuracy, it is limited in its application. The shear amount of data can be restraining the interpretation by overloading the computer. Also the point cloud only offers coordinates at the scanned points and not over a comprehensive model. By further post-processing the three-dimensional point cloud is converted into a digital elevation model which provides data over the whole surface. Prior to the convertion unwanted points (vegetation, etc.) have to be removed from the point cloud. Otherwise they would corrupt the DEM result. By adding the coloured images of the site to the DEM a virtual outcrop model (VOM) is created.

Both the DEM and the VOM can be used for the interpretation and identification of different geological features, such as the orientation of discontinuities.

3.2.3. CONCLUSION

LiDAR scans are used to generate a three-dimensional model of a site (Figure 5). This model can either consist of a three-dimensional point cloud or a meshed surface (DEM). By adding a true-colour image on top of the DEM a virtual outcrop model (VOM) is created. DEMs and VOMs allow the analysation of geological features over wide areas, which are often not easy to access. If necessary the data is referenced to a global coordinate system.

Figure 5: Example of an outcrop and the generated DEM (Liu, 2016).

Therefore the results of a LiDAR survey can be used as input data for the application of block theory on natural rock slopes as shown in this master thesis. It allows the identification of block moulds and the determination of the input parameters joint orientation, spacing and to some extend the friction angle directly from the DEM or VOM.

In contrast to classic geological mapping this allows the analysis of a block mould at a specific location. But LiDAR surveys are still more time and cost intensive compared to geological mapping. Prior to the LiDAR survey the work flow has to be determined accurately. Also the post-processing needs more experience and time in comparison to classic mapping.

3.3. PHOTOGRAMMETRY

3.3.1. GENERAL

Before the invention and common use of LiDAR for the acquisition of geological data photogrammetry had been the only method to collect three-dimensional data over large areas.

In Campell and Wynne (2011) photogrammetry is described as *"the science of making accurate measurements from photographs"*.

3.3.2. DATA ACQUISITION AND POST-PROCESSING

There are different ways to gain the necessary photographs, either airborne, by satellites or ground-based. Independent of the type of data acquisition different types of photographs and thereby information can be taken. The classic application of photogrammetry is done with colour images. In addition infra-red or multi-spectral images can be taken to gain more information (Waltham, 2009). The following interpretation of geology is based on three factors (Waltham, 2009):

- **Tone:** *generally related to water content of soil and plants; dark = wet clay; light = dry sand.*
- **Texture:** *includes drainage channel density and patterns; rock banding and lineations; patchy or mottled ground.*
- **Trend:** *single linear features or correlated anomalies, may trace geological boundaries or structures.*

The position of the camera determines the possible collected data. A clear line of sight as well as the orthogonal arrangement of the camera to the site are necessary. Therefore different positions for image taking should be chosen to guarantee a good coverage and a high quality of the collected data.

Without reference of the location, orientation and size of the site the gained data cannot be used for geological interpretation.

The most important step is the calibration of the used camera. Otherwise the taken images cannot be positioned relatively to each other and the three-dimensional effect is lost. Today automatic calibration of the camera and a measure rod in the image (or any other object with known length) for scaling is state-of-the-art and used for modern surveys.

Using tie points, which can be distinctive points on the site or might be placed there during the photograph is taken, the images are referenced relatively to each other. At least three overlapping points have to be in each photograph. By using for example RTK-GPS to determine the absolute positon of the camera and the tie points the images are positioned absolutely in space.

The referenced models are used for the interpretation and identification of different geological features, such as the orientation of discontinuities.

3.3.3. CONCLUSION

Nowadays photogrammetry can be used to generate a three-dimensional model of a site, which allows the analysis of geological features over wide areas (Figure 6). If necessary the data is referenced to a global coordinate system.
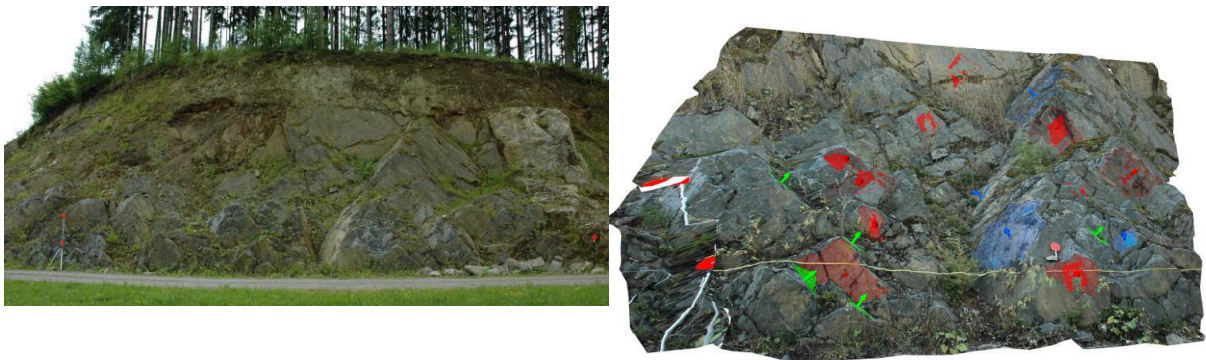
Figure 6: Example of an outcrop (Liu, 2016) and the photogrammetry model (Ahmetovic et al., 2015).

Therefore the results of a photogrammetry survey can be used as input data for the application of block theory on natural rock slopes in the same way LiDAR can be used. It allows the identification of block moulds and the determination of the input parameters joint orientation, spacing and to some extend the friction angle.

In contrast to classic geological mapping this allows the analysis of block moulds at a specified location, same as with LiDAR. In comparison to LiDAR surveys the post-processing is not as time extensive and easier to handle. The biggest disadvantage of photogrammetry is the required free view to the site. Occlusions from vegetation, fog, etc. cannot be remodelled completely by post-processing. Therefore the determination of the work flow of the survey has to be done, as for LiDAR, accurately before starting the survey.

3.4. TRADITIONAL MAPPING (GEOLOGICAL COMPASS, MEASURING TAPE)

Dip and dip direction of a plane can be measured by using a geologic compass.

A compass consists of an inclination measurement plate which is hold against the measured plane (Figure 7). The dip direction is read from the compass and the dip angle is read from the vertical circle. It is important that the circular spirit level is balanced during the measurement.

In addition to the orientation of the joint planes the spacing can be measured easy with a measuring rod. Since the measurement is done on the block mould itself no correction of the spacing regarding the angle of view is needed.

Classic geological mapping is the method with the least data processing since the data is gained directly from the measurement.

Compared to other methods it is easy to execute, no post-processing of data is necessary and vegetation is no handicap. On the other hand less data is gained in the same time, it is not as accurate as for example LiDAR and the slope has to be accessible.
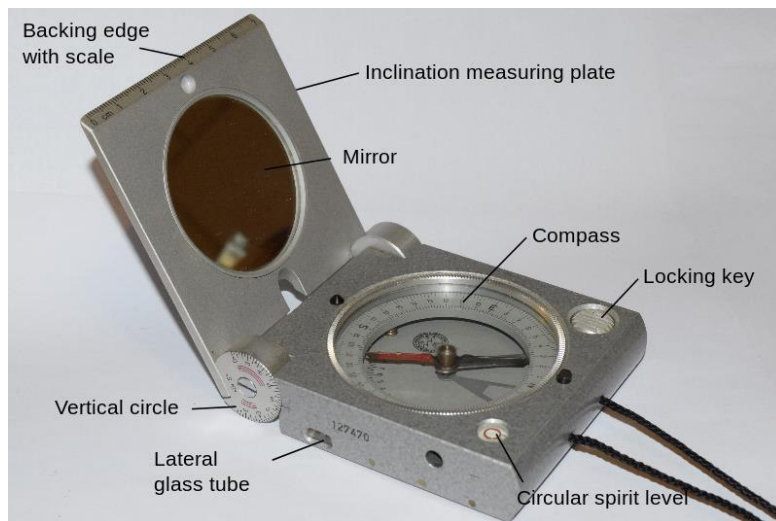
Figure 7: Geological compass ("Wikipedia - Geological compass," 2015).

4. APPLICATION OF BLOCK THEORY ON NATURAL ROCK SLOPES

4.1. GENERAL

In the following chapters the application of block theory for the rapid identification of hazardous blocks in a natural rock slope is described. For the following description and visualisation a block mould in Marhof, Stainz (chapter 5.2) was used.

4.2. IDENTIFICATION OF BLOCK MOULDS IN A NATURAL ROCK SLOPE AND DETERMINATION OF THEIR HALF-SPACE-CODES (JP- AND BP-CODES)

4.2.1. GENERAL

For the analysis of block moulds with block theory the joint orientation, spacing and friction angle are needed. This data can be gained through different types of investigation (chapter 3).

Prior to the analysis with block theory the block has to be identified and its half-space-code must be determined in the field or later on in the office with three-dimensional data from LiDAR or photogrammetry.

4.2.2. IDENTIFICATION OF JOINTS AND FREE PLANES

Block moulds are formed by already failed blocks on a rock slope or at an excavation site. These moulds consist of at least four planes (Figure 3). It is important to distinguish between joint and free planes. Joint planes are still in place and form the mould. The free planes are virtual planes which have formed the block, before it has failed.

Figure 8 shows a block mould in Marhof, Stainz which is comprised of the three governing joint sets KF1 (blue), KF2 (red) and SF (green). Each joint set contributes a joint plane (KF1, KF2, SF) and a free plane (KF1´, KF2´, SF´).

Figure 8: Block mould on a natural rock slope and the governing joint sets KF1 (blue), KF2 (red) and SF (green) which comprise the block.

4.2.3. DETERMINATION OF HALF-SPACE-CODES (JP- AND BP-CODE)

The JP-code defines a potential block and its position relative to the joint planes. In combination with the free planes (EP-code) it forms the BP-code. A block is determined by the two half-spaces a joint or free plane creates in three-dimensional space. It can be either in the upper or in the lower half-space of a plane. This means it is above (upper half-space) or below (lower half-space) the joint or free plane. To shorten the JP-code the upper half-space is represented by 0 and the lower one by 1.

To find the BP-code the block is visualised in Figure 8 on the right side. The block is in the upper half-space (above = 0) of the joint planes KF1 and KF2 and of the free plane SF´. On the other hand the block is in the lower half-space (below = 1) of the joint planes KF1´and KF2´ and the free plane SF. The BP- code of the block is formed as shown in Table 3.

Table 3: Determination of the half-space-codes of the block in Figure 8.

HALF-SPACE-CODES	JOINT PLANES			FREE PLANES		
	KF1	KF2	SF	KF1´	KF2´	SF´
	0	0	1	1	1	0
	JP-code			EP-code		
	001			110		
	BP-code					
	001∩110					

4.3. RECONSTRUCTION AND VISUALISATION OF BLOCK MOULDS WITH BLOCK THEORY

4.3.1. GENERAL

The next step is the reconstruction and visualisation of the block moulds found in the natural rock slope with the parameters joint orientation and spacing.

In this study the programs B02HPGL and B03HPGL (Liu, 2004a, 2004b) were used. These programs are based on block theory (Goodman and Shi, 1985) and were written by Dr. Qian Liu (2004a, 2004b).

4.3.2. RECONSTRUCTION WITH THE PROGRAM B02HPGL

The program B02HPGL (Liu, 2004a) is used to identify potential keyblocks and their type of failure. The input parameters are:

- Number of joint planes
- Number of free planes
- Joint orientation
- Type of stereographic projection
  - lower hemisphere projection: 0,0,-1
  - upper hemisphere projection: 0,0,1
- Direction of the resultant force vector
- Window ratio (1: largest reference circle, 5: smallest reference circle)

If the orientation of a free plane is the same as that of a joint plane, the orientation of the free plane has to be modified slightly, since the computer program cannot process two planes with the same orientation. In Figure 9 an example is shown, where the dip direction of the virtual free planes had been changed by 5 ° in comparison to the joint planes (chapter 5).

The output of B02HPGL are two .plt files (= graphic files), which can be processed by most graphic programs. The first output file is used to identify potential keyblocks and the second one is used to identify the type of failure. In Figure 9 the first output file of the block mould in Marhof Stainz from chapter 4.2 with the BP-code 001∩110 is shown. In Figure 10 the second output file for the same block is shown.

Using lower hemisphere projection the upper half-space is represented by the area outside a great circle. The lower half-space is represented by the area inside a great circle of a joint plane. The area with the half-space-code 001 (JP-code) is highlighted in red. The area of the free space = SP (half-space-code 001) is highlighted in green. The SP is complementary to the EP (half-space-code 110).

After Shi´s Theorem (Goodman and Shi, 1985) only blocks whose JP is totally included in the SP are finite and potentially removable.

Since the red area (JP) is included in the green area (SP) the block is finite and therefore removable.
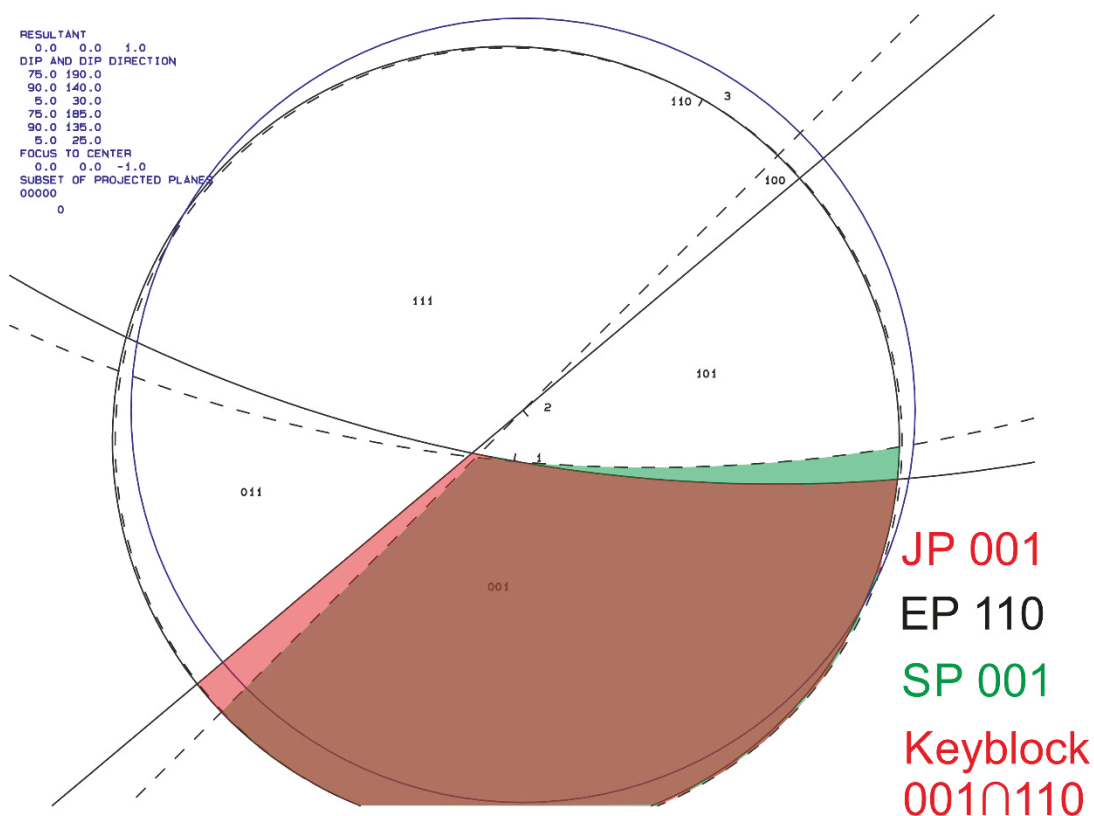
Figure 9: First output file of the program B02HPGL. The Area of the JP-half-space-code 001 is highlighted in red, the area of the free space (half-space-code 001) is highlighted in green. The area of the EP is the white area complementary to the SP.

In Figure 10 the area of the JP with the half-space-code 001 is highlighted in red again. The number inside the area of the JP is the number of the failure plane. In this case it is plane 1 (KF1), which means the block has failed by sliding along plane 1 (KF1).

If there are two numbers inside the JP area, the block failed by wedge sliding along these two planes. For example wedge sliding along plane 1 and plane 2 is represented within the JP-area by 12.
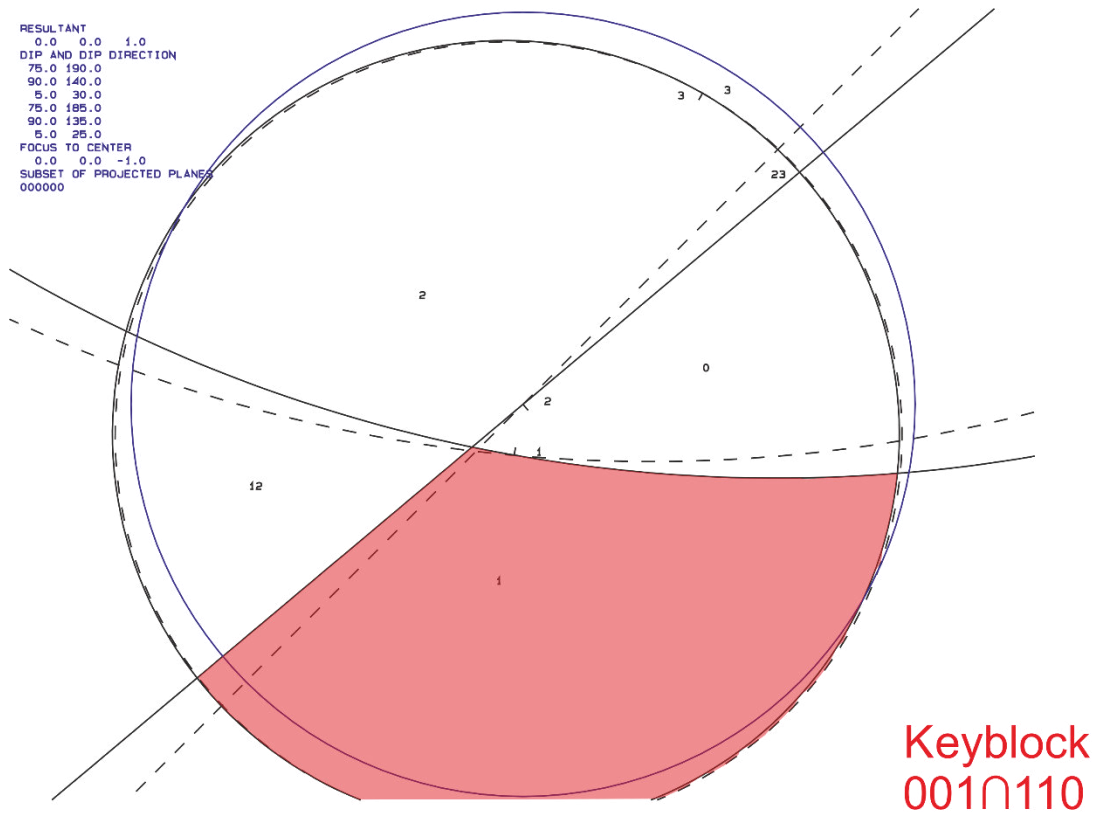
Figure 10: Second output file of the program B02HPGL. The area of the JP-half-space-code 001 is highlighted in red. The number inside the red area is the number of the failure plane. The block mould failed by sliding on plane 1 (KF1).

4.3.3. VISUALISATION WITH THE PROGRAM B03HPGL

The program B03HPGL (Liu, 2004b) is used to visualise blocks. The input parameters are:

- Number of joint planes
- Number of free planes
- Joint orientation
- Joint spacing in meter
    - The actual input value is the half of the real joint spacing. The edge length of a cube is 1.0 m for example, but the input value for B03HPGL would be 0.5 m.
- Direction of projective vector with
    - X … East
    - Y … North
    - Z … Up
- Half-space-code of the block

As with the program B02HPGL (chapter 4.3.2) the orientation of the joint and free planes have to differ in dip direction or dip angle. An example is shown in Figure 11 where the dip direction of the virtual free planes had been changed by 5 ° in comparison to the joint planes (chapter 5).

The output of B03HPGL is also a .plt file (= graphic file), same as with the program B02HPGL. In Figure 11 the output file of the block mould in Marhof, Stainz from chapter 4.2 with the BP-code 001∩110 is shown. For comparison the block mould is shown on the right.

The visualised block is defined by six planes. Three of them still exist as joint planes in nature and are highlighted in blue (plane 1), red (plane 2) and green (plane 3). The free planes (planes 4-6) are virtual planes which formed the block before it had failed.
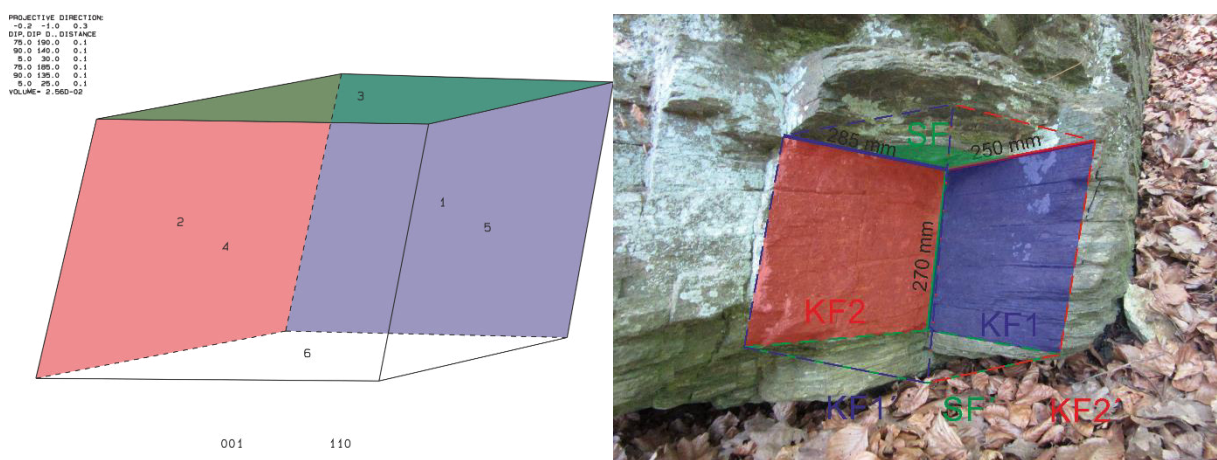
Figure 11: Output file of the program B03HPGL (left) in comparison to the block mould in nature (right). The half-space-code of the visualised block is 001∩110. The joints are highlighted in both images in the same colours for easier understanding.

4.4. IDENTIFICATION AND CHARACTERISATION OF BLOCK FORMING JOINT SETS

4.4.1. GENERAL

For the next step of analysis the joint sets have to be characterised. One of the main input parameter for the analysis with block theory is the friction angle.

The friction angle is usually estimated in field. For non-cohesive joint fillings a friction angle of 30 ° is realistic (Wietek, 2011).

Using the program B04HPGL (Liu, 2004c) a stability analysis of the block can be done. The output is the required friction angle for the block to be stable. The program B09HPGL (Liu, 2004d) is used to display the available friction angle in comparison to the required friction angle.

4.4.2. STABILITY ANALYSIS

The programs B04HPGL and B09HPGL (Liu, 2004c, 2004d) are used for stability analysis. The input parameters are:

- Number of joints on which the block fails
    - 1: planar sliding
    - 2: wedge sliding
- Joint orientation
- JP-code of the block
- Type of stereographic projection
    - lower hemisphere projection: 0,0,-1
    - upper hemisphere projection: 0,0,1
- Step of degrees which is displayed (only B04HPGL)
- Friction angle of the joint(s) (only B09HPGL)
- Window ratio (1: largest reference circle, 5: smallest reference circle)
- Direction of the resultant force vector

The output of B04HPGL and B09HPGL are .plt files (= graphic files), which can be processed by most graphic programs. The output file of B04HPGL shows the required friction angle for the block to be stable. The output file of B09HPGL shows the required friction angle in comparison to the available friction angle. In Figure 12 both output files for the block mould in Marhof, Stainz from chapter 4.2 with the BP-code 001∩110 are shown.

In this case the required friction angle (R) is 75 ° and higher than the available friction angle of 30 °. Therefore the block had failed in nature.
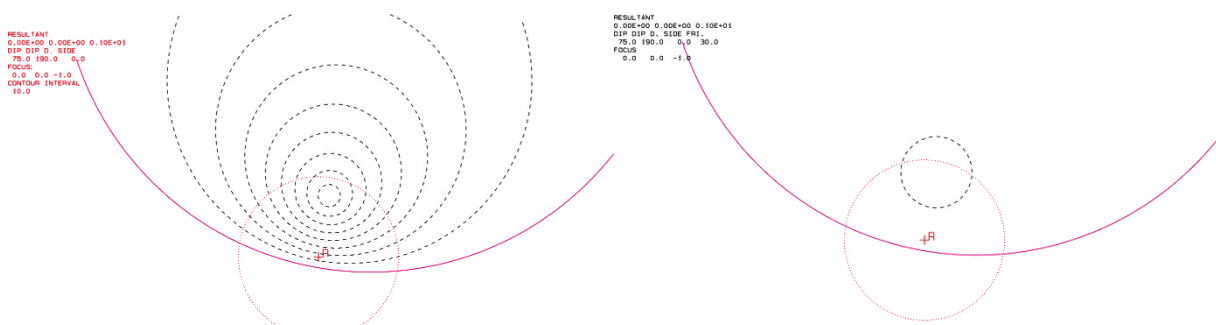
Figure 12: The output file of B04HPGL (left) shows the required friction angle (R). The outputfile of B09HPGL (right) shows the required friction angle (R = 75 °) and the available friction angle (dashed circle = 30 °). The dashed circles are the friction angles, the red circle is a friction angle of 90 °. The required friction angle is represented by R (in red).

4.5. DIFFERENT TYPES OF UNSTABLE BLOCKS IN A NATURAL ROCK SLOPE

4.5.1. GENERAL

In the last step the identified unstable blocks are listed. This list of different types of unstable blocks can be used to anchor the keyblocks and stabilize an entire rock slope.

4.5.2. DIFFERENT TYPES OF UNSTABLE BLOCKS

In the former chapters the block mould 1 from Marhof, Stainz had been used to describe the application of block theory on natural rock slopes.

In Marhof, Stainz two different types of block moulds had been identified in the field (chapter 5.2 and Figure 13). The most common block type had been the block 001∩110.
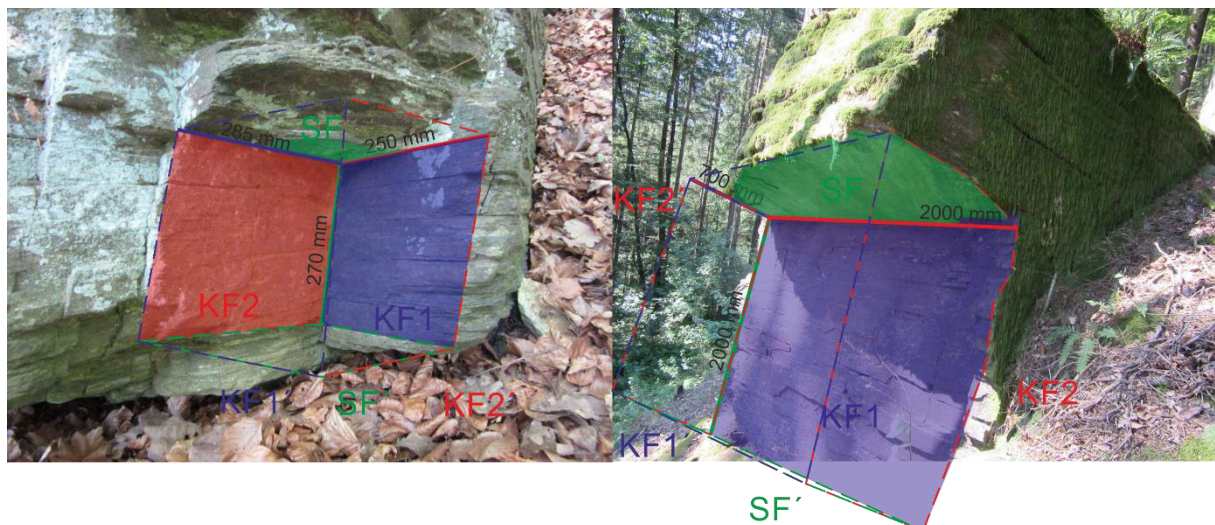
Figure 13: Two different types of unstable blocks in Marhof, Stainz. Block 001∩110 (left) and block 01∩1100 (right).

5. FIELD STUDY

5.1. GENERAL

In the following chapters block theory was applied on two different natural rock slopes. The used methodology is described in chapter 4.

The programs B02HPGL and B03HPGL had been used to identify keyblocks and to visualise those blocks. By using the programs B04HPGL and B09HPGL the stability parameter of each mould had been computed.

In addition to the block specific input parameters (joint orientation, spacing, etc.) the boundary conditions of the analysis are listed below (Table 4).

Table 4: General input parameter for the programs B02HPGL, B03HPGL, B04HPGL, B09HPGL.

PARAMETER	INPUT (X, Y, Z)
Lower hemisphere projection	0,0,-1
Resultant force vector	0,0,-1

The projective vector for visualisation of the blocks had been choosen similar to the angle of view of the photograph taken in field.

5.2. MARHOF, STAINZ (STYRIA, AUSTRIA)

5.2.1. GENERAL

The first rock slope is about 5 km northwest of the city Stainz in Western Styria (Figure 14). The project location is right next to the well "Bad Sauerbrunn". It is on the orographic left side of the Trogbach and the Stainzbach.

Figure 14: Geographical overview, location of the rock slope circled in red. Section of the ÖK 1:50.000, 189 Deutschlandsberg from Digitaler Atlas der Steiermark (Land Steiermark, 2017).

The rock slope in Marhof does not consist of one continuous slope but actually of many small outcrops which are distributed over a large area. The whole outcrop extends over a distance of about 300 m and covers a height of about 60 m. In Figure 15 two smaller outcrops are shown.

Figure 15: Rock slope near Marhof, Stainz.

5.2.2. GEOLOGY

Geologically the project site is situated within the middle austroalpine nape. The outcrops of this study are build up from gneiss, so-called "Stainzer Plattengneis", which belongs to the polymetamorphic base (Figure 16). The rock is characterized by a narrow foliation which originates in multiple metamorphoses and high tectonic stress. In addition extensive joint sets were developed within the rock.

Furthermore "tertiary" (=neogene) and quaternary deposits as talus material can be found in the surroundings of the site.

No.	Formation	Tectonic Subdivison
1	Stainzer Plattengneis	Polymetha-morphic Base
2	Marmor	
3	Gneis, Glimmerschiefer i.a. / Gneisquarzit	
4	Granatglimmerschiefer	
5	Schwanberger Blockschutt	Tertiary
6	Limnisch/fluviatile Entwicklung i.a.: Tone, Mergel,	
7	Hangschutt, Schutthalden	Quaternary
8	Moor, Torf, Sumpf, Vernässung	
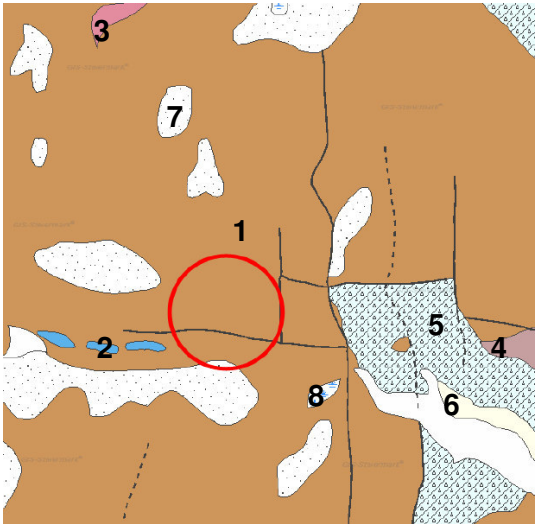
Figure 16: Geological overview, location of the rock slope circled in red. Section of the geological map 1:50.000, 189 Deutschlandsberg from Digitaler Atlas der Steiermark (Land Steiermark, 2017). Geological legend adopted after Digitaler Atlas der Steiermark (Land Steiermark, 2017).

5.2.3. IDENTIFICATION, RECONSTRUCTION AND VISUALISATION OF BLOCK MOULDS

5.2.3.1. MOULD 1

In Figure 17 block mould 1 in Marhof, Stainz is shown. The joint planes are highlighted in blue (KF1), red (KF2) and green (SF). The virtual free planes (KF1´, KF2´, SF´) are also displayed.

The JP-code is 001 (above KF1 and KF2, below SF), the EP-code is 110 (below KF1´ and KF2´, above SF´). Therefore the BP-code of the block mould is 001∩110.
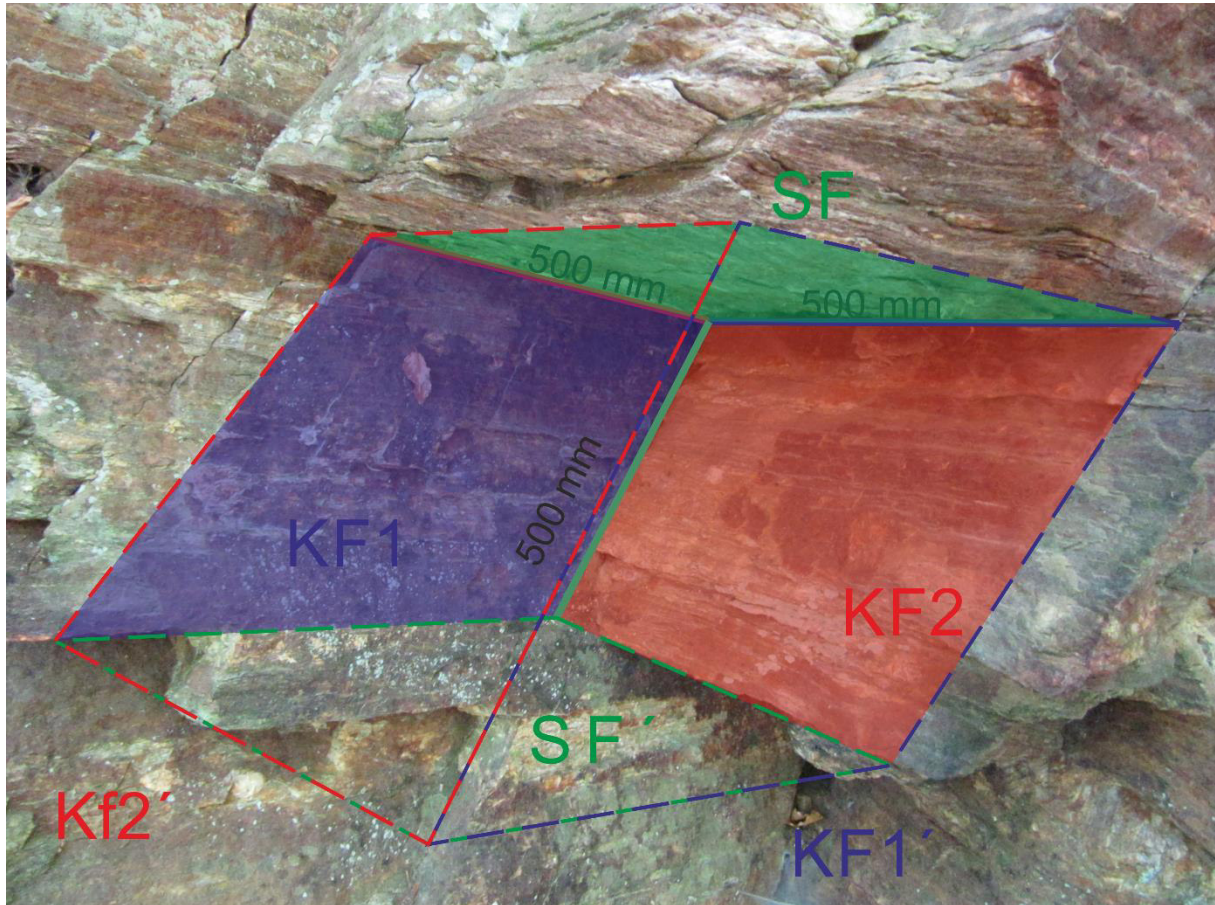

Figure 17: Mould 1 (Marhof, Stainz), showing all joints and free planes.

In Table 5 and Figure 17 the input parameters for the following analysis are shown.

Table 5: Mould 1 (Marhof, Stainz), dip angle and dip direction of joints and free planes [°], joint spacing [m].

	JOINTS	DIP ANGLE / DIP DIRECTION [°]		FREE PLANES	DIP ANGLE / DIP DIRECTION [°]	JOINT SPACING [M]	
1	KF1	75 / 190	4	KF1´	75 / 185	l_{KF1}	0.29
2	KF2	90 / 140	5	KF2´	90 / 135	l_{KF2}	0.25
3	SF	05 / 030	6	SF´	05 / 025	l_{SF}	0.27

Using Figure 18 (first output file of B02HPGL) the corresponding keyblock to the BP-code was identified (highlighted in red). JP = SP can be seen as fulfilled since the dip direction for the free planes was set 5° less than the corresponding joint plane. On that account the analysed block mould was identified as a keyblock by block theory. Figure 19 (second output file of B02HPGL) shows the keyblock and its failure mode, in this case sliding along plane 1 (KF1).
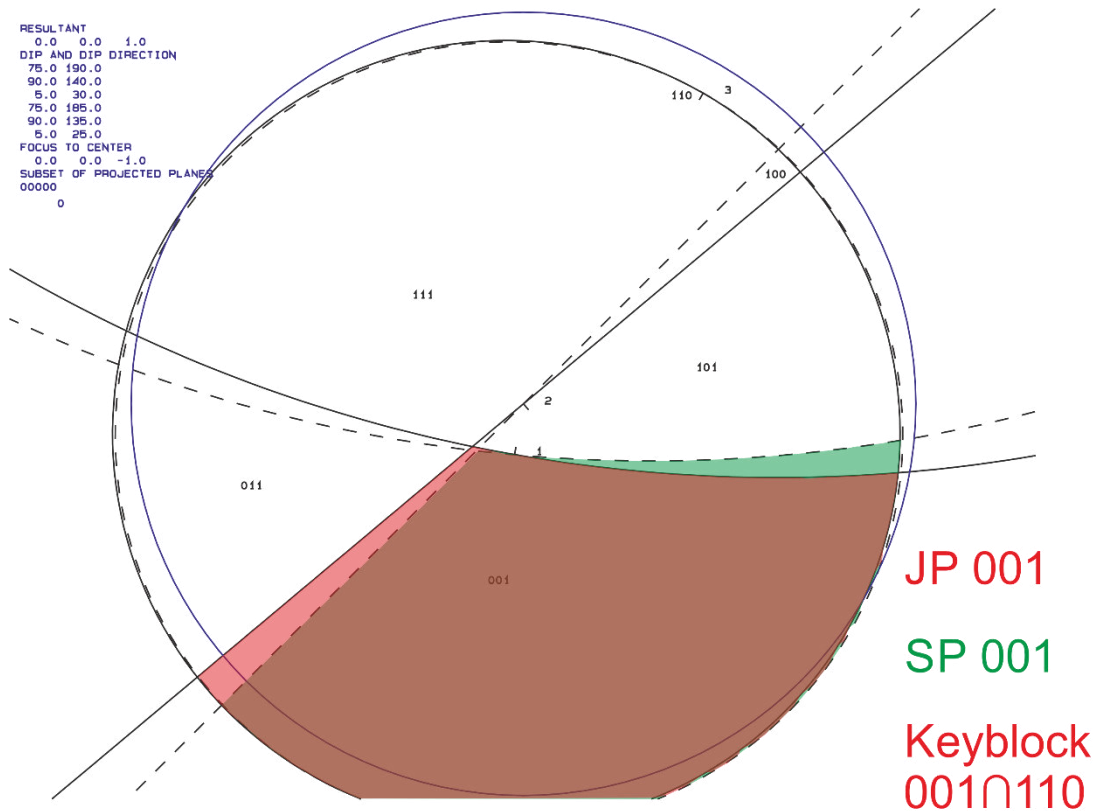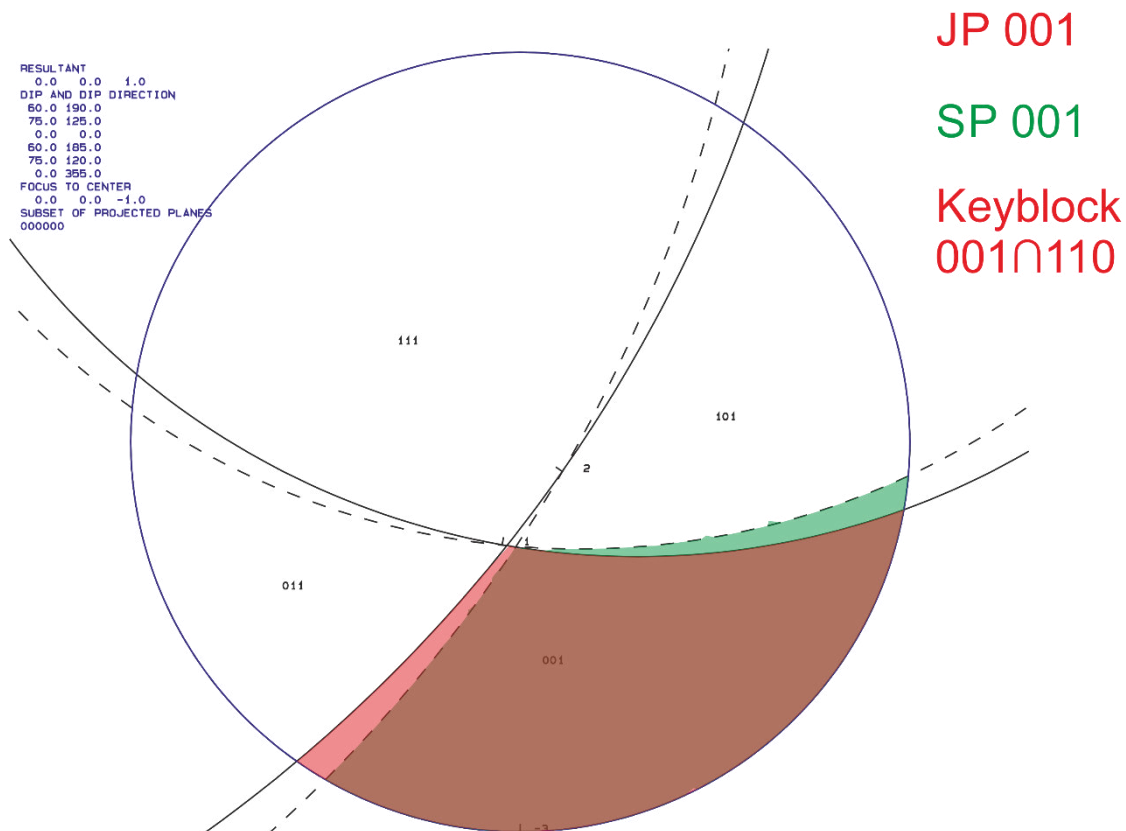

Figure 18: Mould 1 (Marhof, Stainz), output B02HPGL: keyblock (red) and space pyramid SP (green).
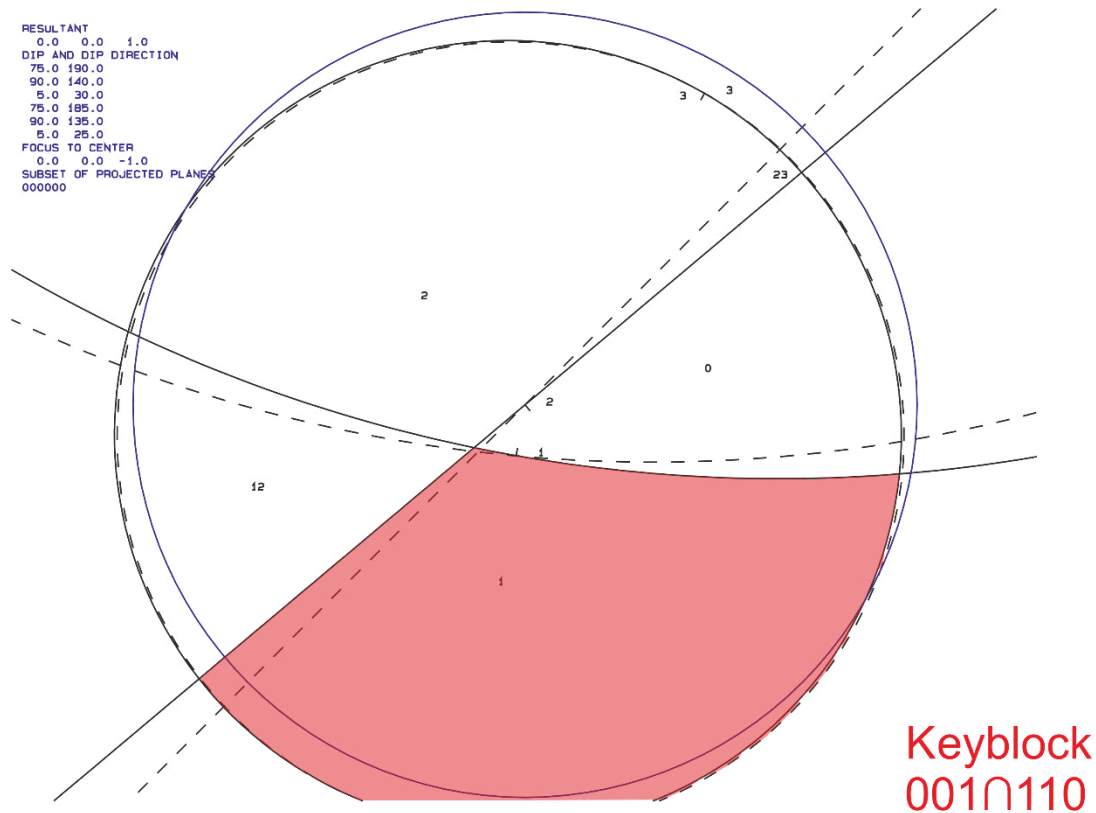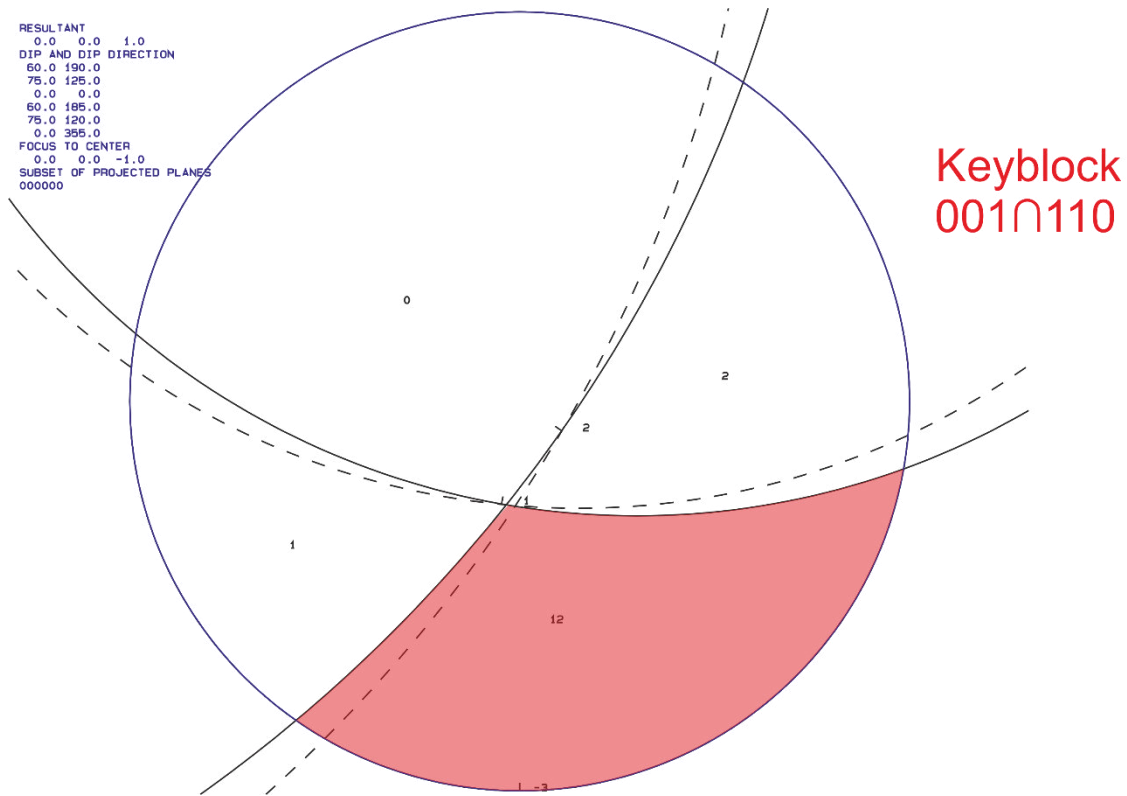
Figure 19: Mould 1 (Marhof, Stainz), output B02HPGL: keyblock (red) and failure plane.

The identified keyblock was visualised with the program B03HPGL (Figure 20). The used input parameters are listed in Table 5 and Table 6. The joint spacing had to be halved for the analysis with B03HPGL. The projective vector represents the view in Figure 17 (Table 6).

Table 6: Mould 1 (Marhof, Stainz), half-space-code and projective vector for B03HPGL.

BLOCK HALF-SPACE-CODE	VIEW NORMAL TO	PROJECTIVE VECTOR (X, Y, Z)
001∩110	KF1	-0.1677, -0.9513, 0.2588

The calculated block volume is 2.56*10^{-2} m^3.

```
PROJECTIVE DIRECTION:
 -0.2  -1.0   0.3
DIP.DIP D.,DISTANCE
 75.0 190.0   0.1
 90.0 140.0   0.1
  5.0  30.0   0.1
 75.0 185.0   0.1
 90.0 135.0   0.1
  5.0  25.0   0.1
VOLUME= 2.56D-02
```
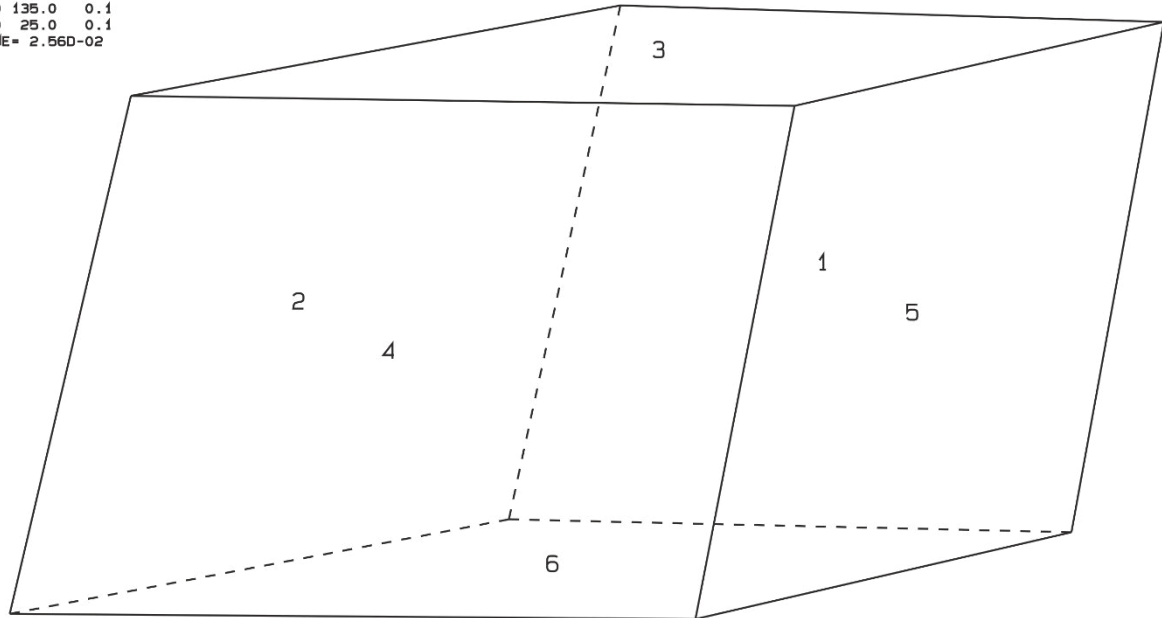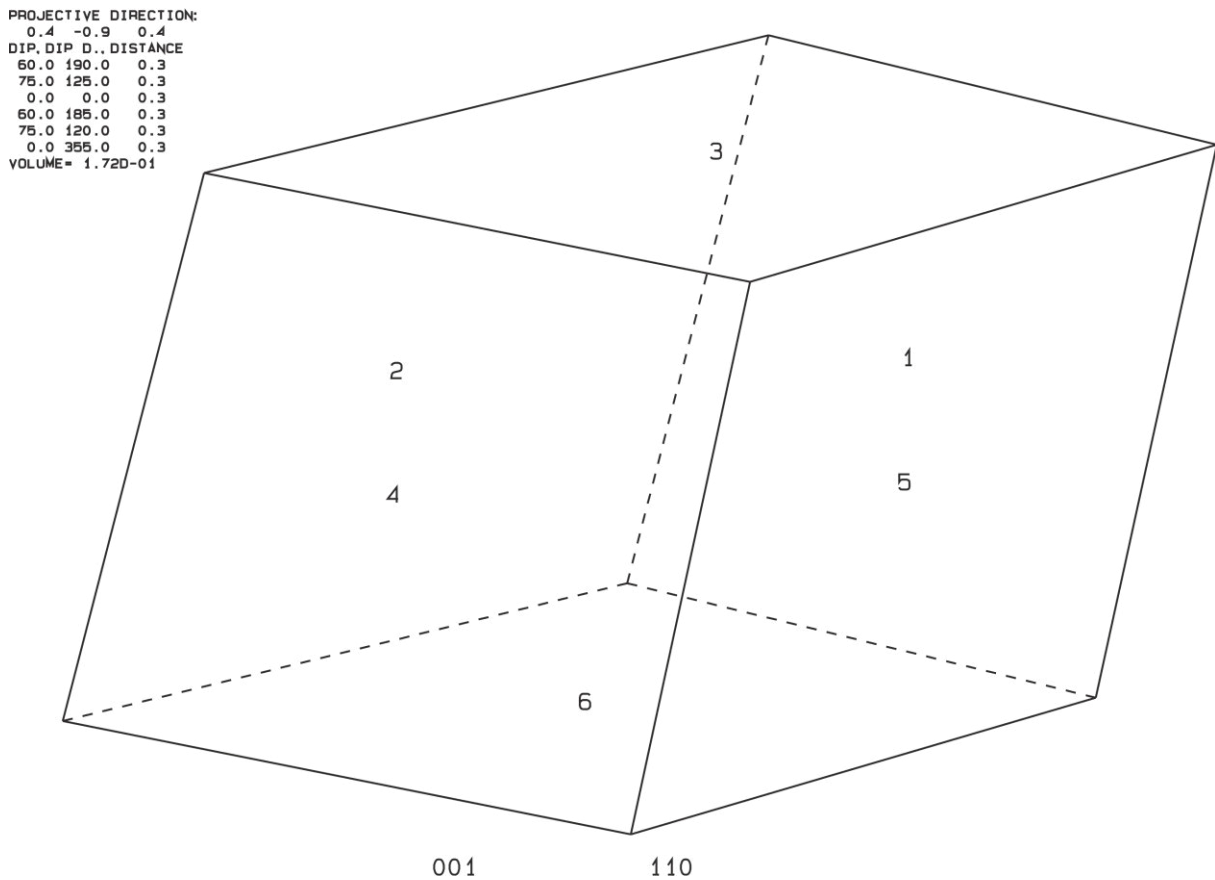

Figure 20: Mould 1 (Marhof, Stainz), block 001∩110 visualized.

5.2.3.2. MOULD 2

In Figure 21 block mould 2 in Marhof, Stainz is shown. The joint planes are highlighted in blue (KF1), red (KF2) and green (SF). The virtual free planes (KF1´, KF2´, SF´) are also displayed.

The JP-code is 001 (above KF1 and KF2, below SF), the EP-code is 110 (below KF1´ and KF2´, above SF´). Therefore the BP-code of the block mould is 001∩110.
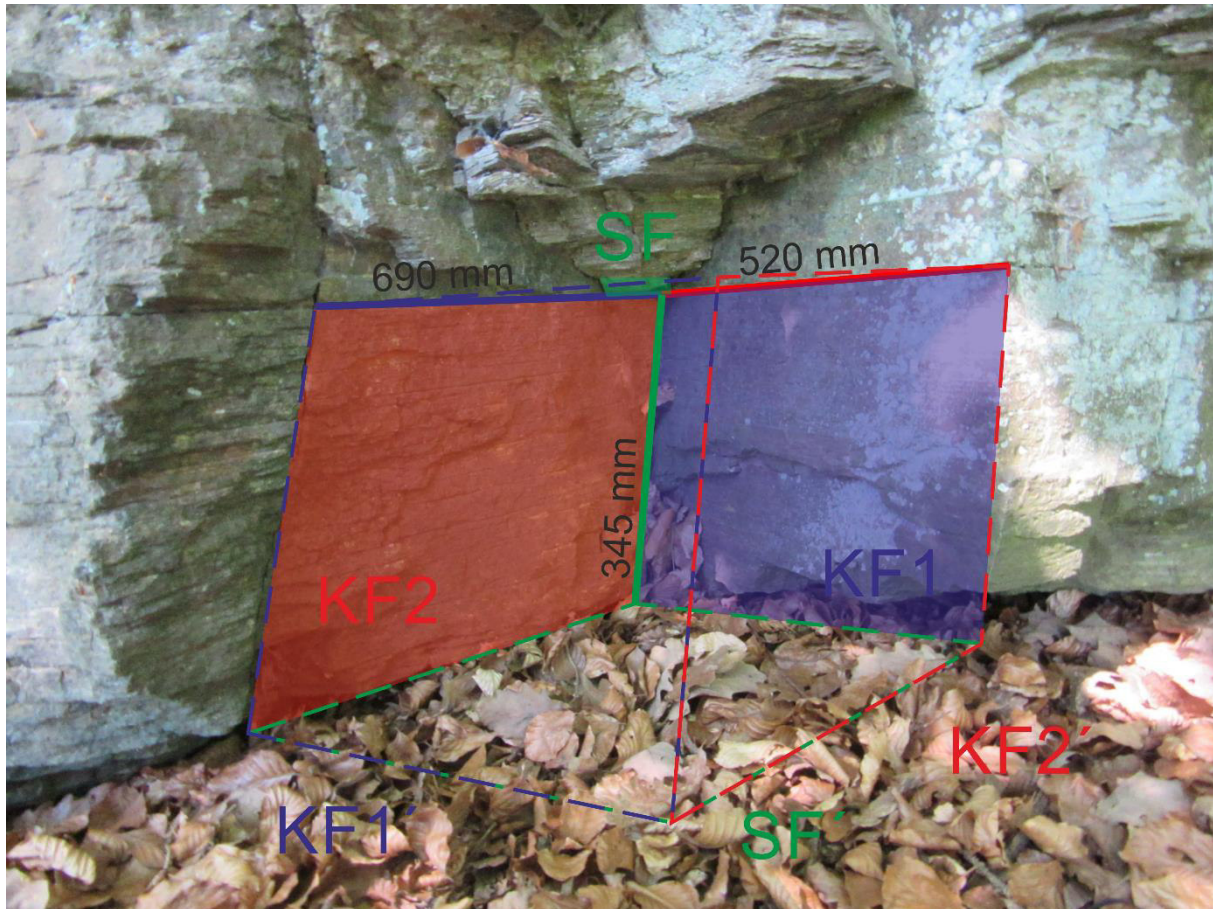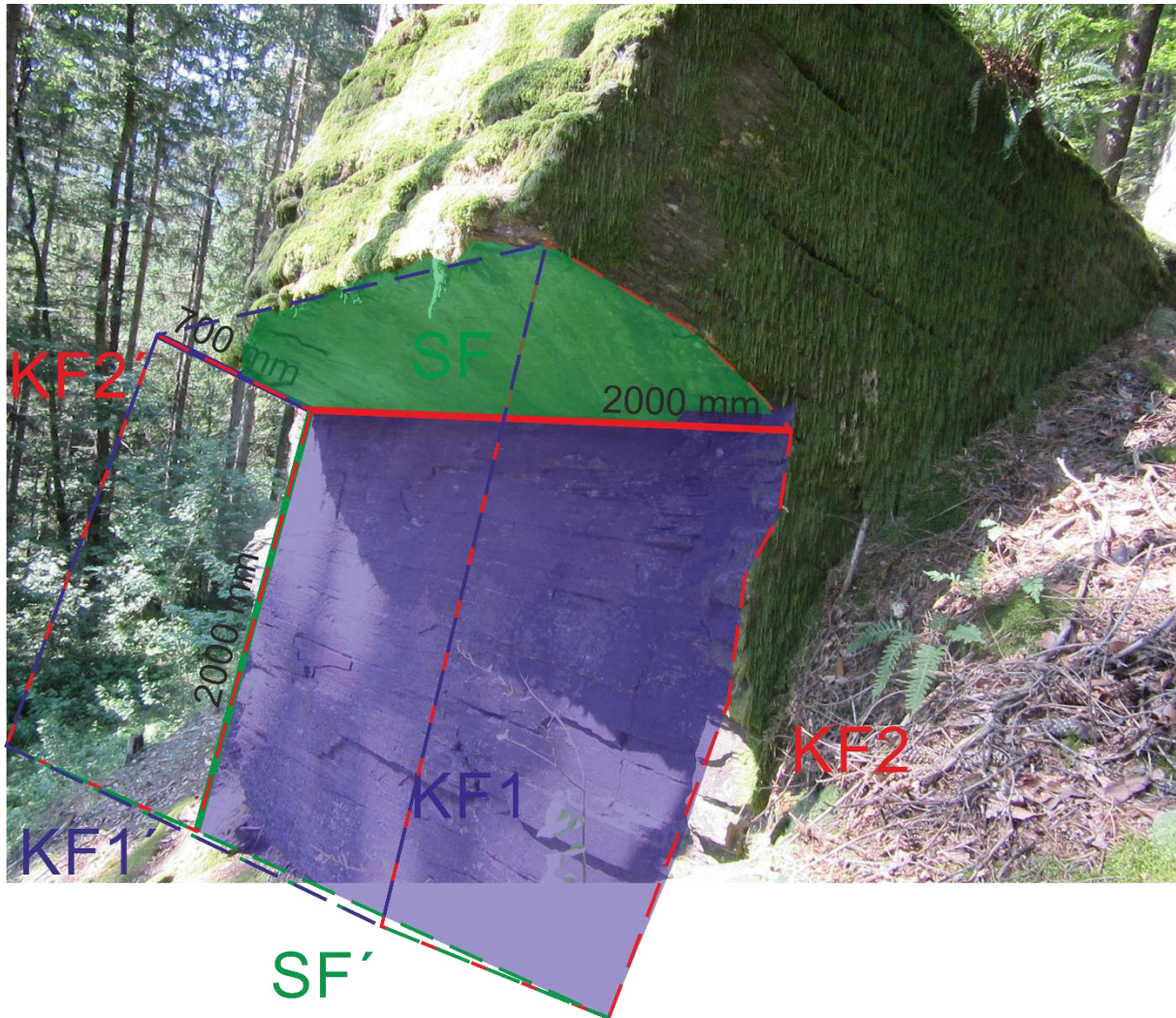
Figure 21: Mould 2 (Marhof, Stainz), showing all joints and free planes.

In Table 7 and Figure 21 the input parameters for the following analysis are shown.

Table 7: Mould 2 (Marhof, Stainz), dip angle and dip direction of joints and free planes [°], joint spacing [m].

JOINTS		DIP ANGLE / DIP DIRECTION [°]	FREE PLANES		DIP ANGLE / DIP DIRECTION [°]	JOINT SPACING [M]	
1	KF1	75 / 235	4	KF1´	75 / 230	l_{KF1}	0.69
2	KF2	85 / 125	5	KF2´	85 / 120	l_{KF2}	0.52
3	SF	05 / 030	6	SF´	05 / 025	l_{SF}	0.35

Using Figure 21 (first output file of B02HPGL) the corresponding keyblock to the BP-code was identified (highlighted in red). JP = SP can be seen as fulfilled since the dip direction for the free planes was set 5° less than the corresponding joint plane. On that account the analysed block mould was identified as a keyblock by block theory. Figure 22 (second output file of B02HPGL) shows the keyblock and its failure mode, in this case wedge sliding along plane 1 (KF1) and plane 2 (KF2).
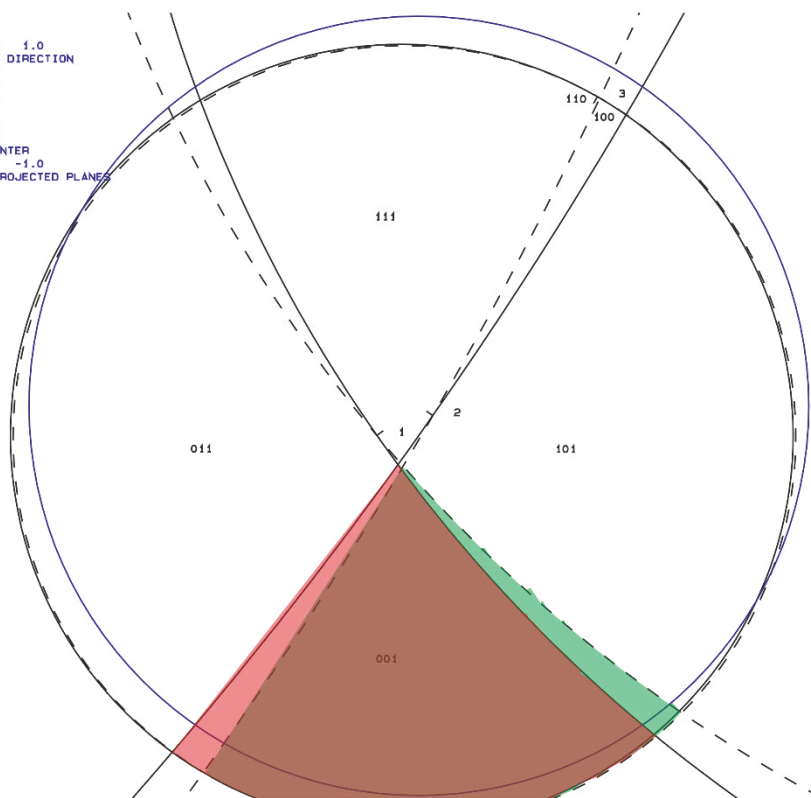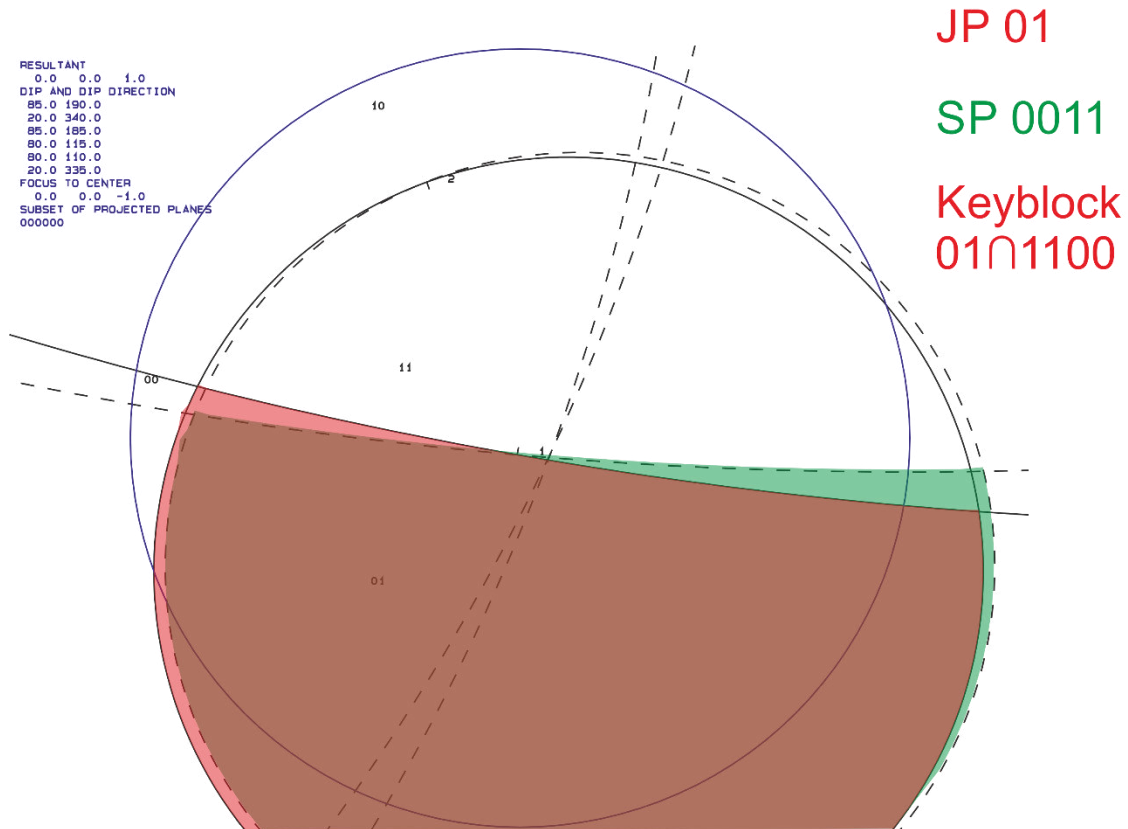
Figure 22: Mould 2 (Marhof, Stainz), output B02HPGL: keyblock (red) and space pyramid SP (green).
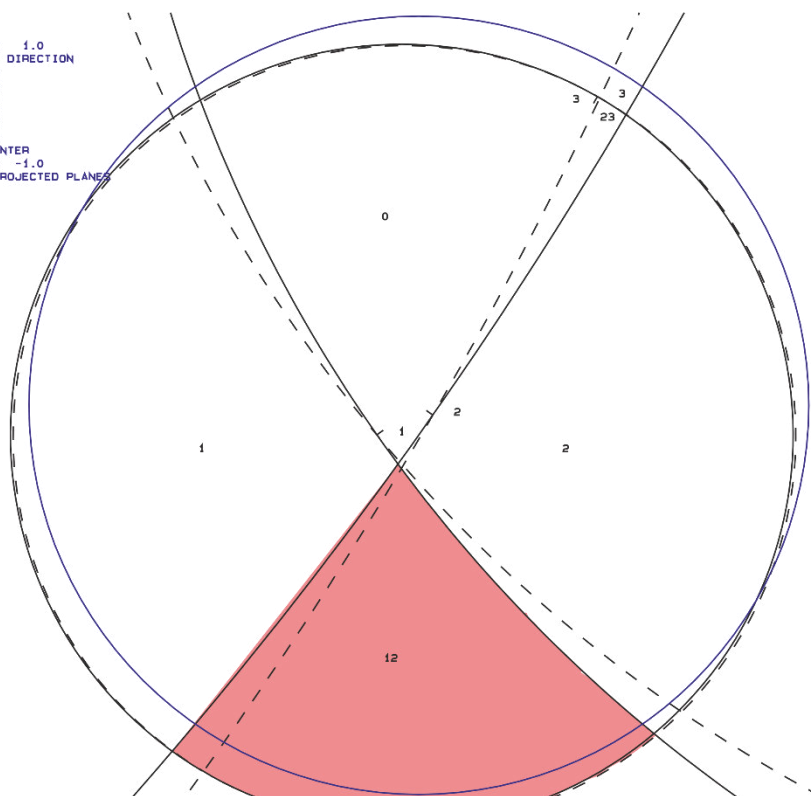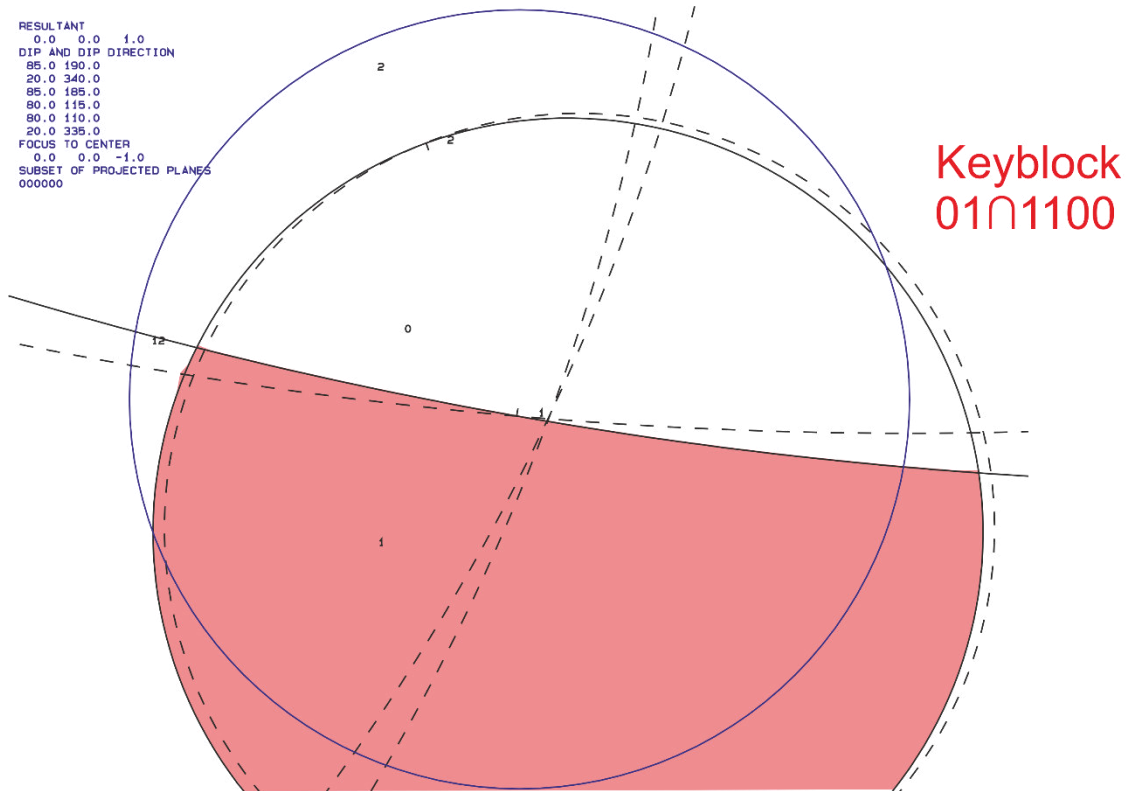

Figure 23: Mould 2 (Marhof, Stainz), output B02HPGL: keyblock (red) and failure plane.

The identified keyblock was visualised with the program B03HPGL (Figure 24). The used input parameters are listed in Table 7 and Table 8. The joint spacing had to be halved for the analysis with B03HPGL. The projective vector represents the view in Figure 21 (Table 8).

Table 8: Mould 2 (Marhof, Stainz), half-space-code and projective vector for B03HPGL.

BLOCK HALF-SPACE-CODE	VIEW NORMAL TO	PROJECTIVE VECTOR (X, Y, Z)
001∩110	Edge KF1 – KF2	0.0, -0.9848, 0.1736

The calculated block volume is $1.34*10^{-1}$ m^3.
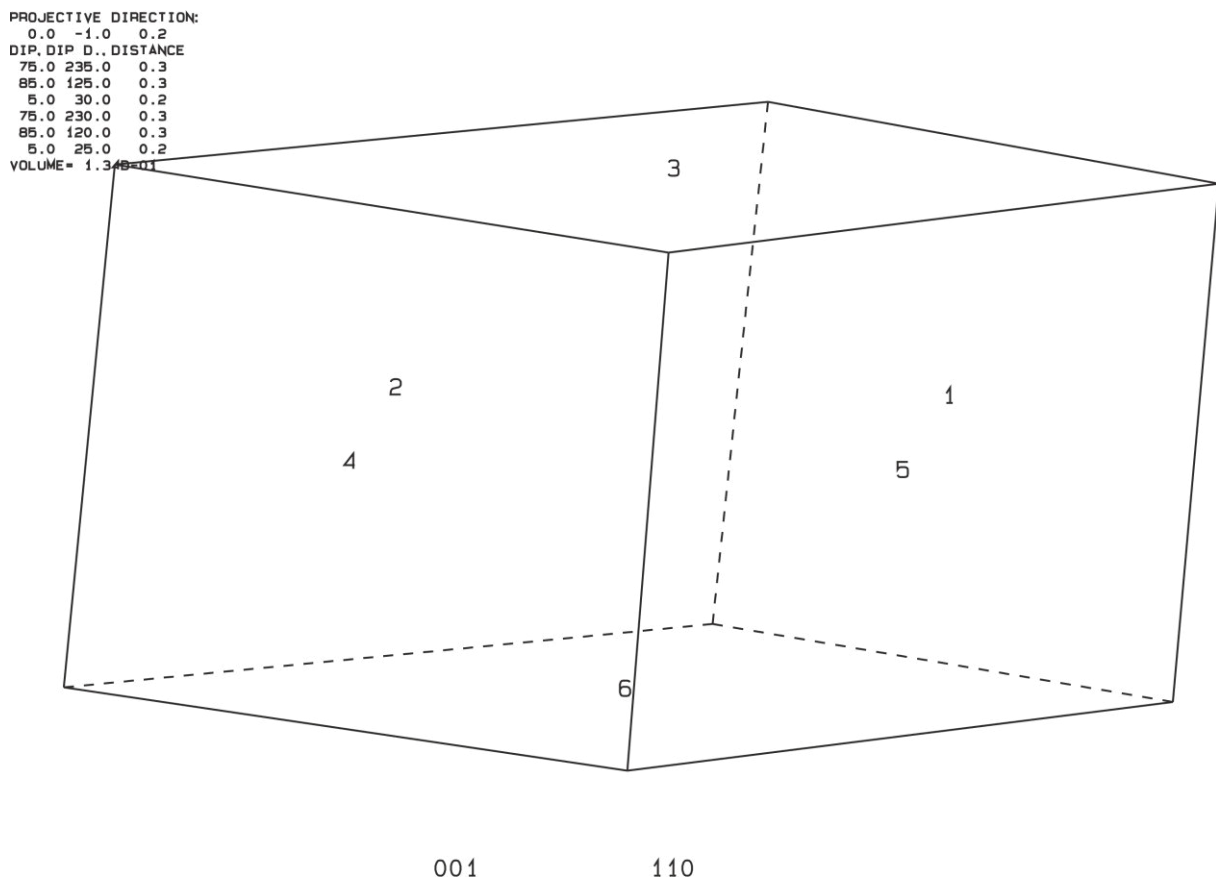
Figure 24: Mould 2 (Marhof, Stainz), block 001∩110 visualized.

5.2.3.3. MOULD 3

In Figure 25 block mould 3 in Marhof, Stainz is shown. The joint planes are highlighted in blue (KF1), red (KF2) and green (SF). The virtual free planes (KF1´, KF2´, SF´) are also displayed.

The JP-code is 001 (above KF1 and KF2, below SF), the EP-code is 110 (below KF1´ and KF2´, above SF´). Therefore the BP-code of the block mould is 001∩110.

Figure 25: Mould 3 (Marhof, Stainz), showing all joints and free planes.

In Table 9 and Figure 25 the input parameters for the following analysis are shown.

Table 9: Mould 3 (Marhof, Stainz), dip angle and dip direction of joints and free planes [°], joint spacing [m].

JOINTS		DIP ANGLE / DIP DIRECTION [°]	FREE PLANES		DIP ANGLE / DIP DIRECTION [°]	JOINT SPACING [M]	
1	KF1	60 / 190	4	KF1´	60 / 185	l_{KF1}	0.50
2	KF2	75 / 125	5	KF2´	75 / 120	l_{KF2}	0.52
3	SF	00 / 000	6	SF´	00 / 355	l_{SF}	0.50

Using Figure 26 (first output file of B02HPGL) the corresponding keyblock to the BP-code was identified (highlighted in red). JP = SP can be seen as fulfilled since the dip direction for the free planes was set 5° less than the corresponding joint plane. On that account the analysed block mould was identified as a keyblock by block theory. Figure 27 (second output file of B02HPGL) shows the keyblock and its failure mode, in this case wedge sliding along plane 1 (KF1) and plane 2 (KF2).

Figure 26: Mould 3 (Marhof, Stainz), output B02HPGL: keyblock (red) and space pyramid SP (green).

Figure 27: Mould 3 (Marhof, Stainz), output B02HPGL: keyblock (red) and failure planes.

The identified keyblock was visualised with the program B03HPGL (Figure 28). The used input parameters are listed in Table 9 and Table 10. The joint spacing had to be halved for the analysis with B03HPGL. The projective vector represents the view in Figure 25 (Table 10).

Table 10: Mould 3 (Marhof, Stainz), half-space-code and projective vector for B03HPGL.

BLOCK HALF-SPACE-CODE	VIEW NORMAL TO	PROJECTIVE VECTOR (X, Y, Z)
001∩110	Edge KF1 – KF2	0.3536, -0.8536, 0.3827

The calculated block volume is $1.72*10^{-1}$ m^3.


```
PROJECTIVE DIRECTION:
  0.4  -0.9   0.4
DIP, DIP D., DISTANCE
 60.0 190.0   0.3
 75.0 125.0   0.3
  0.0   0.0   0.3
 60.0 185.0   0.3
 75.0 120.0   0.3
  0.0 355.0   0.3
VOLUME= 1.72D-01
```

Figure 28: Mould 3 (Marhof, Stainz), block 001∩110 visualized.

5.2.3.4. MOULD 4

In Figure 29 block mould 4 in Marhof, Stainz is shown. The joint planes are highlighted in blue (KF1) and green (SF). The virtual free planes (KF1´, KF2, KF2´, SF´) are also displayed.

The JP-code is 01 (above KF1, below SF), the EP-code is 1100 (below KF1´ and KF2, above KF2´ and SF´). Therefore the BP-code of the block mould is 01∩1100.

Figure 29: Mould 4 (Marhof, Stainz), showing all joints and free planes.

In Table 5 and Figure 17 the input parameters for the following analysis are shown.

Table 11: Mould 4 (Marhof, Stainz), dip angle and dip direction of joints and free planes [°], joint spacing [m].

	JOINTS	DIP ANGLE / DIP DIRECTION [°]		FREE PLANES	DIP ANGLE / DIP DIRECTION [°]	JOINT SPACING [M]	
1	KF1	85 / 190	3	KF1´	85 / 185	I_{KF1}	0.70
2	SF	20 / 340	4	KF2	80 / 115	I_{KF2}	2.00
			5	KF2´	80 / 110	I_{SF}	2.00
			6	SF´	20 / 335		

Using Figure 30 (first output file of B02HPGL) the corresponding keyblock to the BP-code was identified (highlighted in red). JP = SP can be seen as fulfilled since the dip direction for the free planes was set 5° less than the corresponding joint plane. On that account the analysed block mould was identified as a keyblock by block theory. Figure 31 (second output file of B02HPGL) shows the keyblock and its failure mode, in this case sliding along plane 1 (KF1).

Figure 30: Mould 4 (Marhof, Stainz), output B02HPGL: keyblock (red) and space pyramid SP (green).

Figure 31: Mould 4 (Marhof, Stainz), output B02HPGL: keyblock (red) and failure plane

The identified keyblock was visualised with the program B03HPGL (Figure 32). The used input parameters are listed in Table 11 and Table 12. The joint spacing had to be halved for the analysis with B03HPGL. The projective vector represents the view in Figure 29 (Table 12).

Table 12: Mould 4 (Marhof, Stainz), half-space-code and projective vector for B03HPGL.

BLOCK HALF-SPACE-CODE	VIEW NORMAL TO	PROJECTIVE VECTOR (X, Y, Z)
01∩1100	KF2	0.8925, -0.4162, 0.1736

The calculated block volume is 2.98 m^3.


```
PROJECTIVE DIRECTION:
  0.9  -0.4   0.2
DIP, DIP D., DISTANCE
 85.0 190.0   0.3
 20.0 340.0   1.0
 85.0 185.0   0.3
 80.0 115.0   1.0
 80.0 110.0   1.0
 20.0 335.0   1.0
VOLUME= 2.98D+00
```
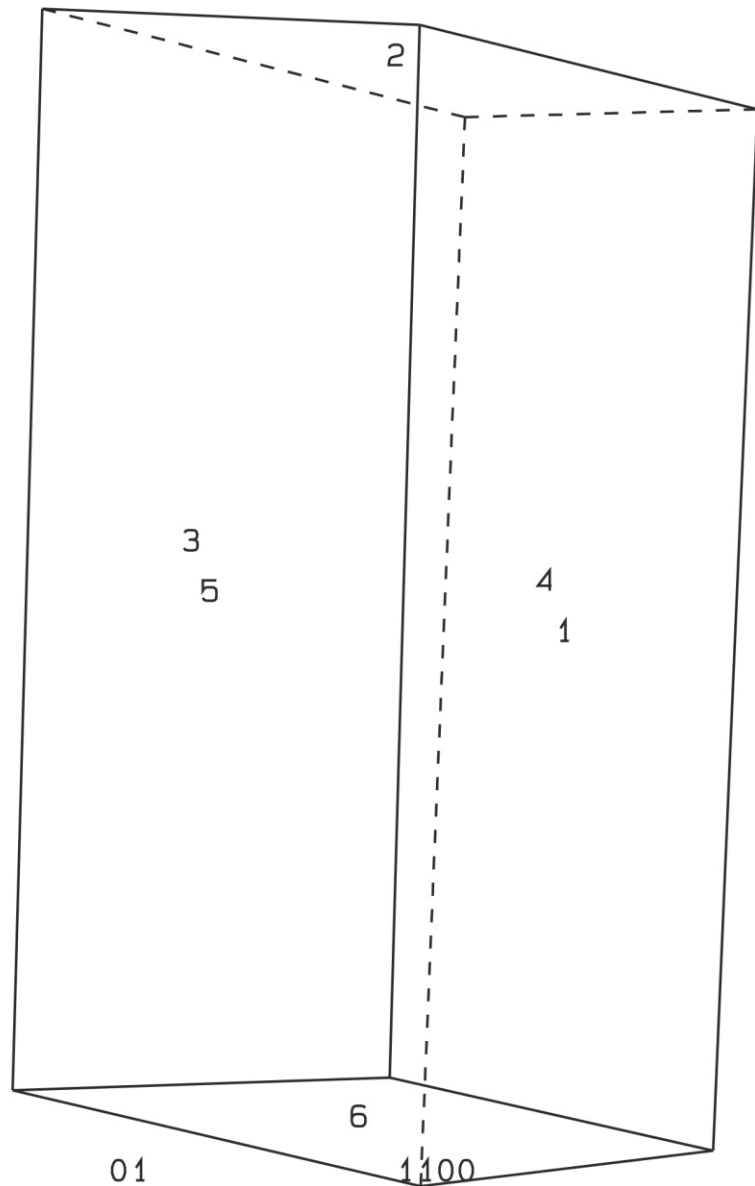
Figure 32: Mould 4 (Marhof, Stainz), block 01∩1100 visualized.

5.2.4. STABILITY ANALYSIS

5.2.4.1. MOULD 1

For stability analysis the programs B04HPGL and B09HPGL were used. The input parameters are listed in Table 13.

Table 13: Mould 1 (Marhof, Stainz), import parameters for B04HPGL and B09HPGL.

JOINTS		DIP ANGLE / DIP DIRECTION [°]	FREE PLANES		DIP ANGLE / DIP DIRECTION [°]	OTHER	
1	KF1	75 / 190	4	KF1´	75 / 185	Friction angle	30 °
2	KF2	90 / 140	5	KF2´	90 / 135	Sliding along	KF1
3	SF	05 / 030	6	SF´	05 / 025	BP-code	001∩110

The required friction angle is 75 ° (marked with R, Figure 33). The available friction angle is only 30 °. Since the required friction angle is higher than the available friction angle the block has failed in nature.
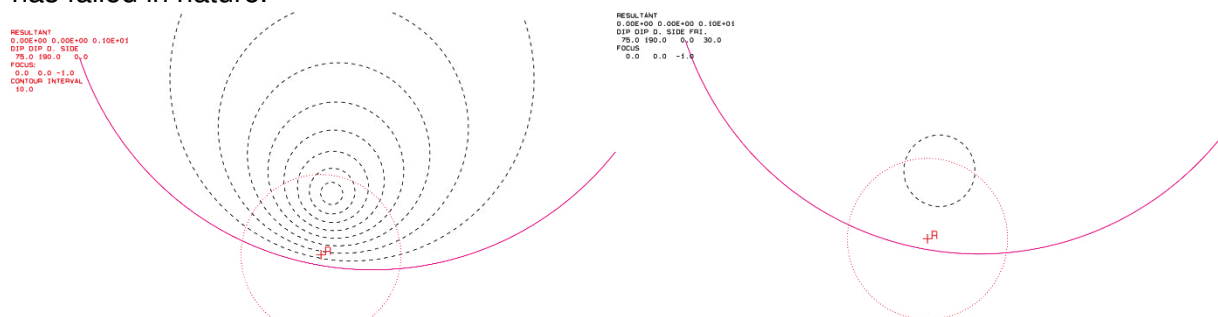
Figure 33: Mould 1 (Marhof, Stainz), output files of B04HPGL and B09HPGL.

5.2.4.2. MOULD 2

For stability analysis the programs B04HPGL and B09HPGL were used. The input parameters are listed in Table 14.

Table 14: Mould 2 (Marhof, Stainz), import parameters for B04HPGL and B09HPGL.

JOINTS		DIP ANGLE / DIP DIRECTION [°]	FREE PLANES		DIP ANGLE / DIP DIRECTION [°]	OTHER	
1	KF1	75 / 235	4	KF1´	75 / 230	Friction angle	30 °
2	KF2	85 / 125	5	KF2´	85 / 120	Sliding along	KF1 & KF2
3	SF	05 / 030	6	SF´	05 / 025	BP-code	001∩110

The required friction angle is 60 ° (marked with R, Figure 34). The available friction angle is only 30 °. Since the required friction angle is higher than the available friction angle the block has failed in nature.
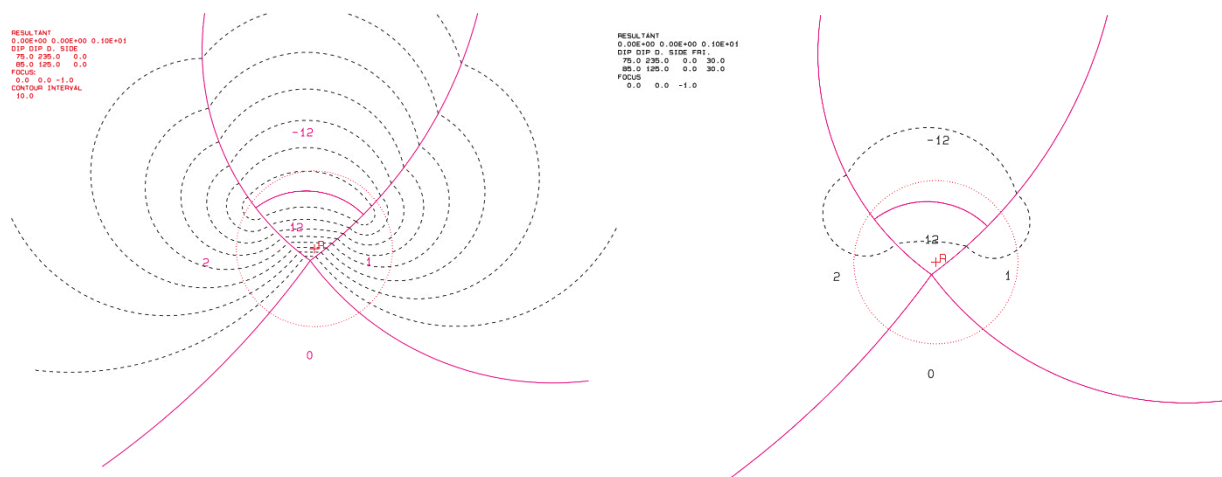
Figure 34: Mould 2 (Marhof, Stainz), output files of B04HPGL and B09HPGL.

5.2.4.3. MOULD 3

For stability analysis the programs B04HPGL and B09HPGL were used. The input parameters are listed in Table 15.

Table 15: Mould 3 (Marhof, Stainz), import parameters for B04HPGL and B09HPGL.

JOINTS		DIP ANGLE / DIP DIRECTION [°]	FREE PLANES		DIP ANGLE / DIP DIRECTION [°]	OTHER	
1	KF1	60 / 190	4	KF1´	60 / 185	Friction angle	30 °
2	KF2	75 / 125	5	KF2´	75 / 120	Sliding along	KF1 & KF2
3	SF	00 / 000	6	SF´	00 / 355	BP-code	001∩110

The required friction angle is 60 ° (marked with R, Figure 35). The available friction angle is only 30 °. Since the required friction angle is higher than the available friction angle the block has failed in nature.
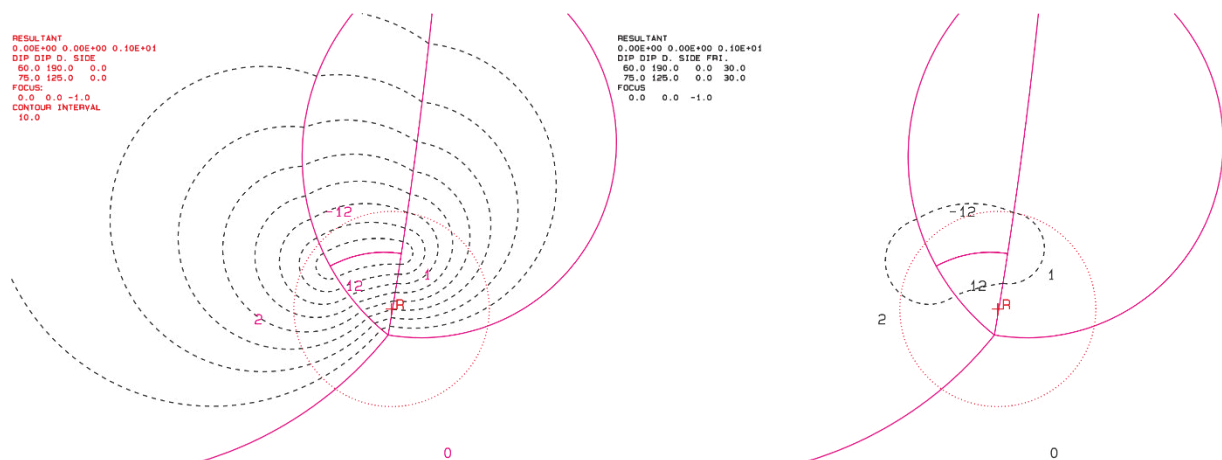
Figure 35: Mould 3 (Marhof, Stainz), output files of B04HPGL and B09HPGL.

5.2.4.4. MOULD 4

For stability analysis the programs B04HPGL and B09HPGL were used. The input parameters are listed in Table 16.

Table 16: Mould 4 (Marhof, Stainz), import parameters for B04HPGL and B09HPGL.

JOINTS		DIP ANGLE / DIP DIRECTION [°]	FREE PLANES		DIP ANGLE / DIP DIRECTION [°]	OTHER	
1	KF1	85 / 190	3	KF1´	85 / 185	Friction angle	30 °
2	SF	20 / 340	4	KF2	80 / 115	Sliding along	KF1
			5	KF2´	80 / 110	BP-code	01∩1100
			6	SF´	20 / 335		

The required friction angle is 85 ° (marked with R, Figure 36). The available friction angle is only 30 °. Since the required friction angle is higher than the available friction angle the block has failed in nature.
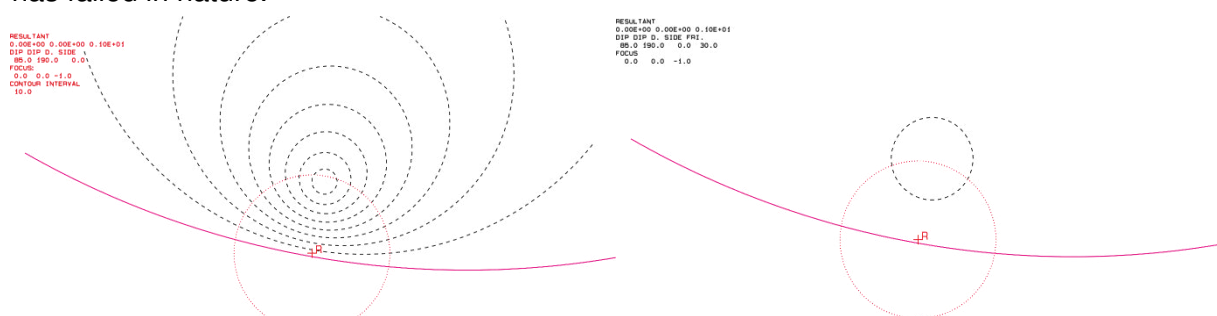
Figure 36: Mould 4 (Marhof, Stainz), output files of B04HPGL and B09HPGL.

5.3. OBERWÖLZ (STYRIA, AUSTRIA)

5.3.1. GENERAL

The second site is about 5 km southeast of the city Oberwölz in Upper Styria (Figure 37). The project location is about 500 m after the junction of the B75 Glattjochstraße to the L514 Hocheggerstraße on the right side. The Schönbergerbach is also right next to it. In Figure 38 the whole rock slope is shown.

Figure 37: Geographical overview, location of the rock slope circled in red. Section of the ÖK 1:50.000, 159 Murau and 160 Neumarkt from Digitaler Atlas der Steiermark (Land Steiermark, 2017).

Figure 38: Rock slope near Oberwölz.

5.3.2. GEOLOGY

Geologically the project site is situated at the boundary between the upper austroalpine and the middle austroalpine nape. The rock slope of this study is build up from carbonate ("Bänderkalk") and accounts to the so-called "Murauer Paläozoikum" which is part of the upper austroalpine (Figure 39). The "Murauer Paläozoikum" is a low metamorphic unit, originally deposited in the Palaeozoic era (Devonian to Carboniferous). The rock is characterised by its brittle behaviour. Below the "Murauer Paläozoikum" rocks of the polymethamorphic base (Middle Austroalpine) are found.

In addition to the solid rock quaternary deposits as alluvial fans can be found in the surroundings of the site.

No	Formation	Tectonic Subdivison
1	Phyllitischer Glimmerschiefer	Polymetha-morphic Base
2	Feldspat-Granatglimmerschiefer	
3	Grünschiefer, z.T. Prasinit	"Murauer Paläozoikum"
4	Kohlenstoffquarzphyllit, Kohlenstoffgranatphyllit	
5	Grauer Kalk, Bänderkalk	
6	Kalke i.a.: Murauer - Pleschaitz - Grebenzenkalk	
7	Grundmoräne	Quaternary
8	Schwemm-/ Schuttfächer, Alluvium	
9	Eisrandterrasse	

Figure 39: Geological overview, location of the rock slope circled in red. Section of the geological map 1:50.000, 159 Murau and 160 Neumarkt from Digitaler Atlas der Steiermark (Land Steiermark, 2017). Geological legend adopted after Digitaler Atlas der Steiermark (Land Steiermark, 2017).

5.3.3. IDENTIFICATION, RECONSTRUCTION AND VISUALISATION OF BLOCK MOULDS

5.3.3.1. MOULD 1

In Figure 40 block mould 1 in Oberwölz is shown. The joint planes are highlighted in red (KF1), yellow (KF2), blue (KF3) and green (BF).

The JP-code is 0001 (above KF1, KF2 and KF3, below BF), the EP-code is 01 (above BF´, below KF3´). Therefore the BP-code of the block mould is 0001∩01.

Figure 40: Mould 1 (Oberwölz), showing all joints and free planes.

In Table 17 and Figure 40 the input parameters for the following analysis are shown.

Table 17: Mould 1 (Oberwölz), dip angle and dip direction of joints and free planes [°], joint spacing [m].

JOINTS		DIP ANGLE / DIP DIRECTION [°]	FREE PLANES		DIP ANGLE / DIP DIRECTION [°]	JOINT SPACING [M]	
1	KF1	67 / 055	5	BF´	20 / 010	l_{KF1}	1.50
2	KF2	60 / 132	6	KF3´	80 / 110	l_{KF2}	1.50
3	KF3	80 / 106				l_{KF3}	0.70
4	BF	20 / 015				l_{BF}	1.00

Using Figure 41 (first output file of B02HPGL) the corresponding keyblock to the BP-code was identified (highlighted in red). JP = SP can be seen as fulfilled since the dip direction for the free planes was set 5° less than the corresponding joint plane. On that account the analysed block mould was identified as a keyblock by block theory. Figure 42 (second output file of B02HPGL) shows the keyblock and its failure mode, in this case wedge sliding along plane 1 (KF1) and plane 2 (KF2).
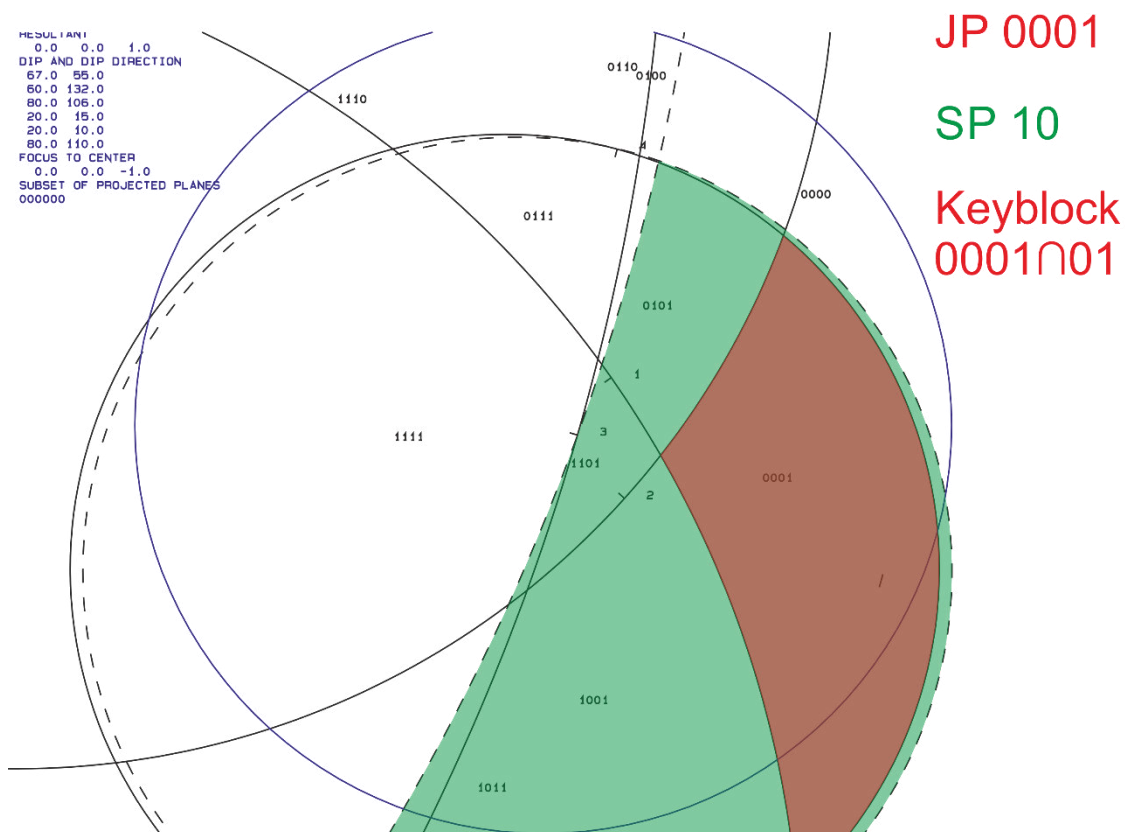
Figure 41: Mould 1 (Oberwölz), output B02HPGL: keyblock (red) and space pyramid SP (green).
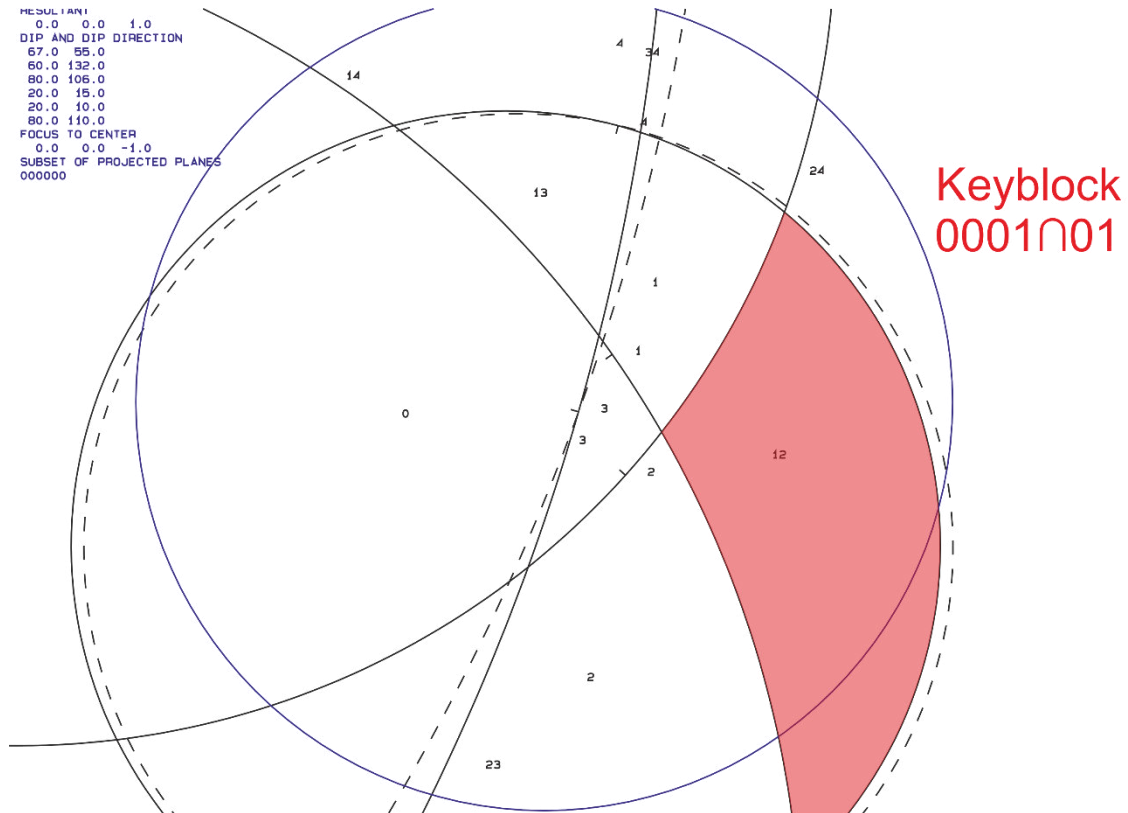
Figure 42: Mould 1 (Oberwölz), output B02HPGL: keyblock (red) and failure planes.

The identified keyblock was visualised with the program B03HPGL (Figure 43). The used input parameters are listed in Table 17 and Table 18. The joint spacing had to be halved for the analysis with B03HPGL. The projective vector represents the view in Figure 40 (Table 18).

Table 18: Mould 1 (Oberwölz), half-space-code and projective vector for B03HPGL.

BLOCK HALF-SPACE-CODE	VIEW NORMAL TO	PROJECTIVE VECTOR (X, Y, Z)
0001∩01	KF3	0.95, -0.27, 0.17

The calculated block volume is 2.11 m³.

```
PROJECTIVE DIRECTION:
  0.9  -0.3   0.2
DIP, DIP D., DISTANCE
 67.0  55.0    0.8
 60.0 132.0    0.8
 80.0 106.0    0.3
 20.0  15.0    0.5
 20.0  10.0    0.5
 80.0 110.0    0.3
VOLUME= 2.11D+00
```
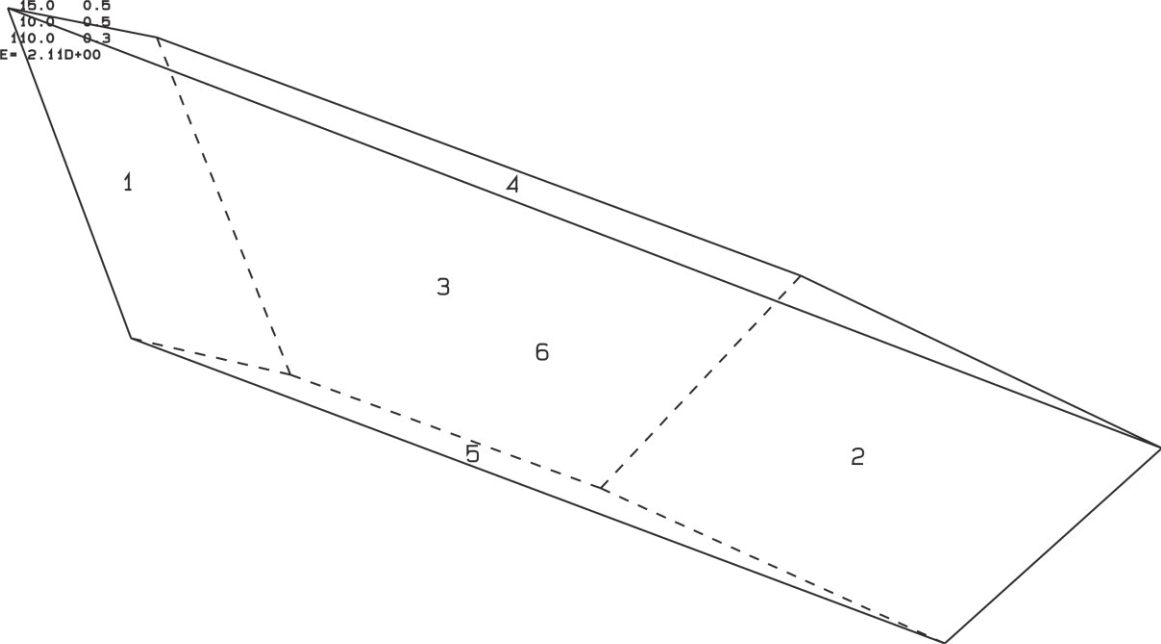
Figure 43: Mould 1 (Oberwölz), block 0001∩01 visualized.

5.3.3.2. MOULD 2

In Figure 44 block mould 2 in Oberwölz is shown. The joint planes are highlighted in red (KF1), yellow (KF2), blue (KF3) and green (BF).

The JP-code is 0001 (above KF1, KF2 and KF3, below BF), the EP-code is 01 (above BF´, below KF3´). Therefore the BP-code of the block mould is 0001∩01.

Figure 44: Mould 2 (Oberwölz), showing all joints and free planes.

In Table 19 and Figure 44 the input parameters for the following analysis are shown.

Table 19: Mould 2 (Oberwölz), dip angle and dip direction of joints and free planes [°], joint spacing [m].

JOINTS		DIP ANGLE / DIP DIRECTION [°]	FREE PLANES		DIP ANGLE / DIP DIRECTION [°]	JOINT SPACING [M]	
1	KF1	65 / 092	5	BF´	30 / 357	l_{KF1}	1.00
2	KF2	75 / 214	6	KF3´	80 / 130	l_{KF2}	1.00
3	KF3	55 / 138				l_{KF3}	0.30
4	BF	30 / 002				l_{BF}	0.30

Using Figure 45 (first output file of B02HPGL) the corresponding keyblock to the BP-code was identified (highlighted in red). Since the dip direction for the free planes were set 5° less than the corresponding joint plane JP = SP can be seen as fulfilled. On that account the analysed block mould was identified as a keyblock by block theory. Figure 46 (second output file of B02HPGL) shows the keyblock and its failure mode, in this case wedge sliding along plane 1 (KF1) and plane 2 (KF2).
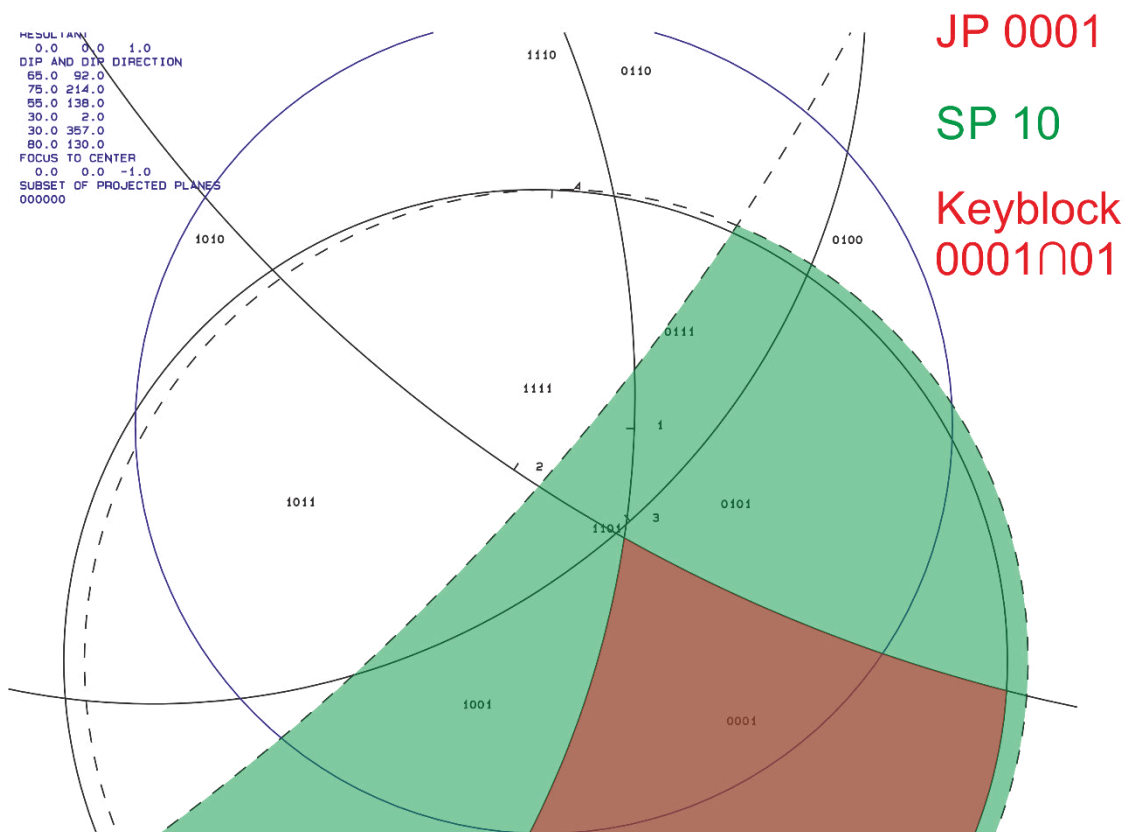
Figure 45: Mould 2 (Oberwölz), output B02HPGL: keyblock (red) and space pyramid SP (green).
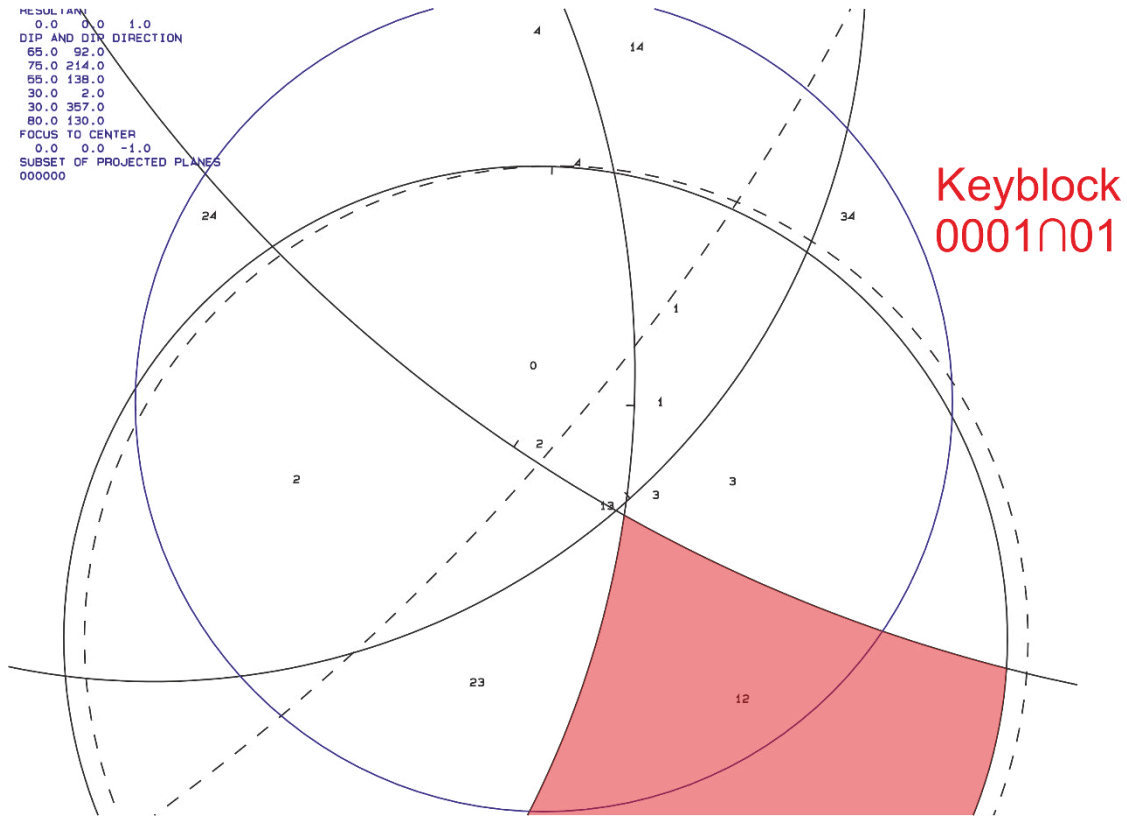
Figure 46: Mould 2 (Oberwölz), output B02HPGL: keyblock (red) and failure plane

The identified keyblock was visualised with the program B03HPGL (Figure 47). The used input parameters are listed in Table 19 and Table 20. The joint spacing had to be halved for the analysis with B03HPGL. The projective vector represents the view in Figure 44 (Table 20).

Table 20: Mould 2 (Oberwölz), half-space-code and projective vector for B03HPGL.

BLOCK HALF-SPACE-CODE	VIEW NORMAL TO	PROJECTIVE VECTOR (X, Y, Z)
0001∩01	KF3	0.55, -0.61, 0.57

The calculated block volume is 1.83*10⁻¹ m³.


```
PROJECTIVE DIRECTION:
   0.6  -0.6   0.6
DIP,DIP D.,DISTANCE
  65.0  92.0   0.5
  75.0 214.0   0.5
  55.0 138.0   0.2
  30.0   2.0   0.2
  30.0 357.0   0.2
  80.0 130.0   0.2
VOLUME= 1.83D-01
```
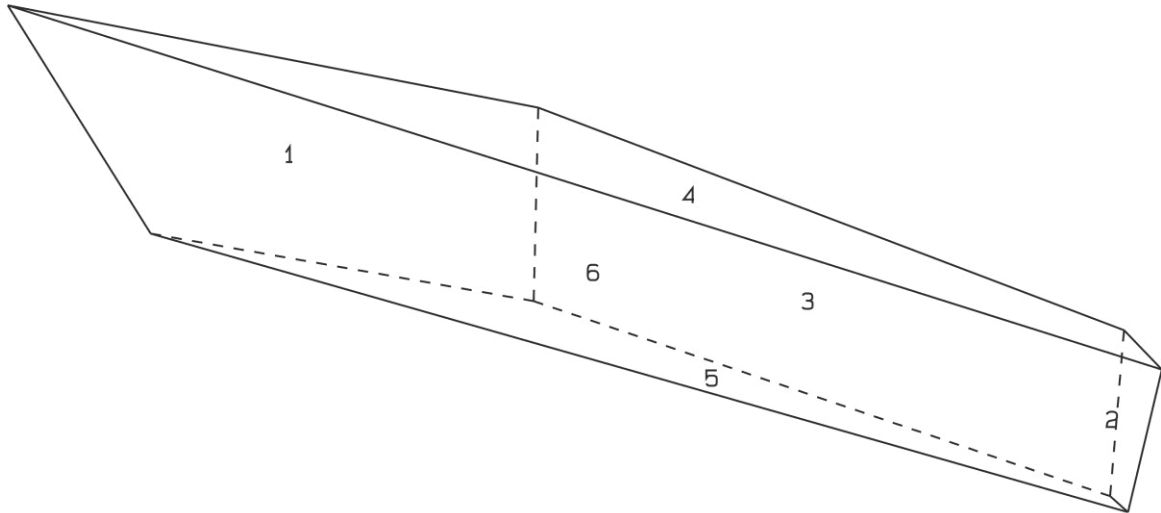
Figure 47: Mould 2 (Oberwölz), block 0001∩01 visualized.

5.3.4. STABILITY ANALYSIS

5.3.4.1. MOULD 1

For stability analysis the programs B04HPGL and B09HPGL were used. The input parameters are listed in Table 13.

Table 21: Mould 1 (Oberwölz), import parameters for B04HPGL and B09HPGL.

JOINTS		DIP ANGLE / DIP DIRECTION [°]	FREE PLANES		DIP ANGLE / DIP DIRECTION [°]	JOINT SPACING [M]	
1	KF1	67 / 055	5	BF´	20 / 010	Friction angle	30 °
2	KF2	60 / 132	6	KF3´	80 / 110	Sliding along	KF1
3	KF3	80 / 106				BP-code	0001∩01
4	BF	20 / 015					

The required friction angle is 50 ° (marked with R, Figure 48). The available friction angle is only 30 °. Since the required friction angle is higher than the available friction angle the block has failed in nature.
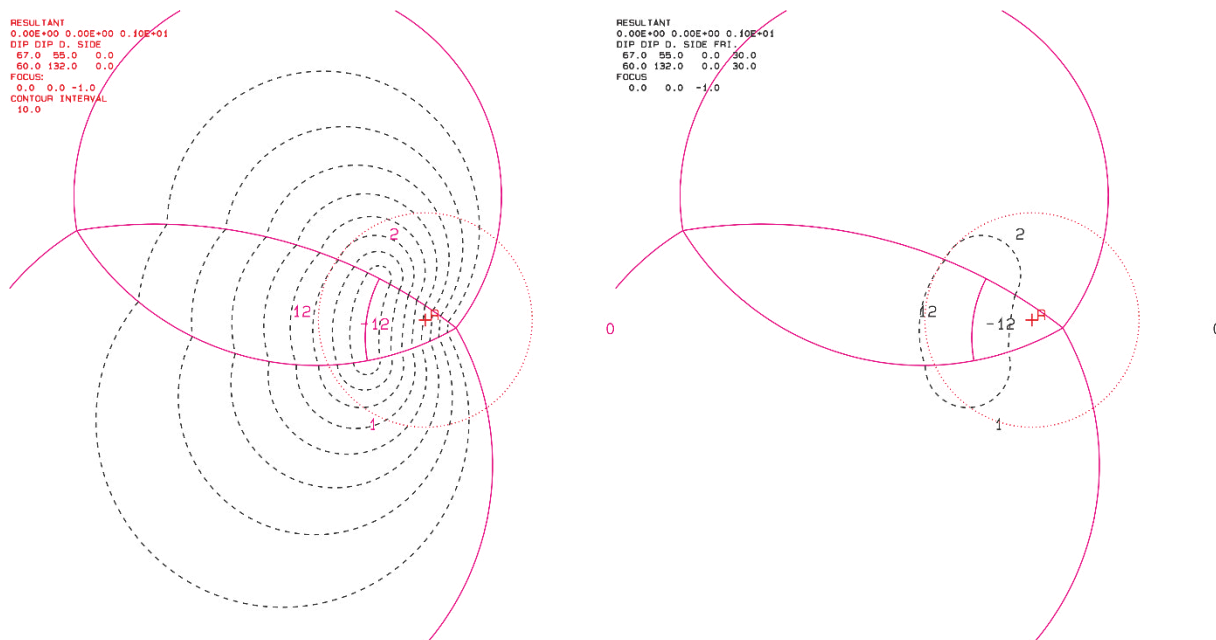
Figure 48: Mould 1 (Oberwölz), output files of B04HPGL and B09HPGL.

5.3.4.2. MOULD 2

For stability analysis the programs B04HPGL and B09HPGL were used. The input parameters are listed in Table 13.

Table 22: Mould 2 (Oberwölz), import parameters for B04HPGL and B09HPGL.

JOINTS		DIP ANGLE / DIP DIRECTION [°]	FREE PLANES		DIP ANGLE / DIP DIRECTION [°]	JOINT SPACING [M]	
1	KF1	65 / 092	5	BF´	30 / 357	Friction angle	30 °
2	KF2	75 / 214	6	KF3´	80 / 130	Sliding along	KF1
3	KF3	55 / 138				BP-code	0001∩01
4	BF	30 / 002					

The required friction angle is 35 ° (marked with R, Figure 49). The available friction angle is only 30 °. Since the required friction angle is higher than the available friction angle the block has failed in nature.
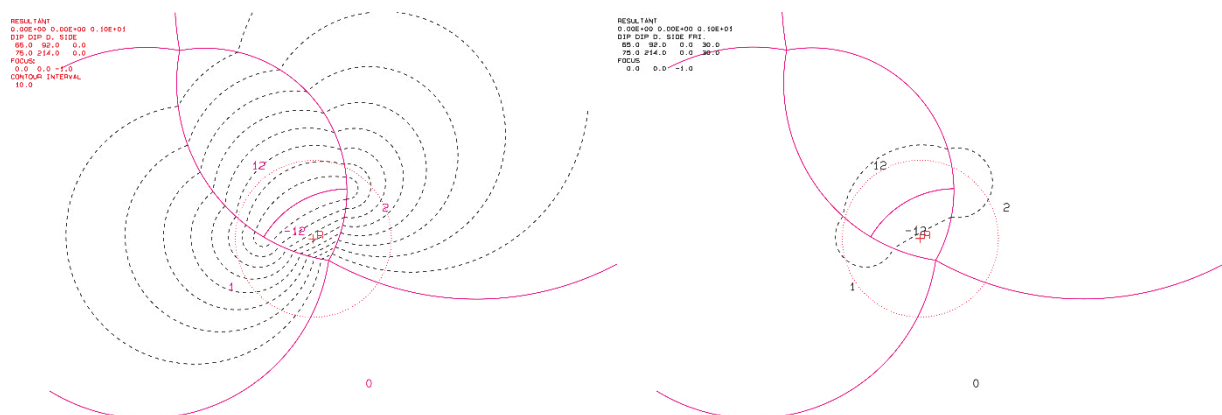
Figure 49: Mould 2 (Oberwölz), output files of B04HPGL and B09HPGL.

5.4. RESULTS

In Marhof, Stainz and Oberwölz different moulds were analysed with block theory. The used methodology is described in chapter 4.

The data was gained by classic geological mapping. During data acquisition in the field the BP-code of each block was determined. In Marhof, Stainz two different types of blocks were identified and analysed and in Oberwölz one type of block was found.

- Marhof, Stainz:
    - 001∩110
    - 01∩1100
- Oberwölz:
    - 0001∩01

All blocks were identified as keyblocks with the program B02HPGL and afterwards visualised with the program B03HPGL (chapter 5.2.3 and 5.3.3). Thereby the block volume was computed.

In the next step the required friction angle was computed and compared to the available friction angle (chapter 5.2.4 and 5.3.4). In all cases the required friction angle was higher than the available friction angle. Therefore the blocks had failed in nature.

The analysed block moulds could have been identified with block theory before they failed. It is shown that block theory can be used for the identification of hazardous blocks on crystalline and carbonate natural rock slopes.

6.   DISCUSSION

In the past different kinds of rock mass classification have been used in engineering geology. But putting a highly complex system as a discontinuous rock mass into simplified categories may lead to wrong conclusions concerning rock behaviour.

After Goodman and Shi (1985) introduced block theory it has been applied on different types of rock and different excavation sites instead of and/or complementary to rock mass classification. On the other hand the usage on natural rock slopes was novel.

In this thesis block theory was applied on natural rock slopes using block moulds. To show its applicability the methodology was tested on two different sites. The input parameters were joint orientation, spacing and friction angle and had been gained by classic geological mapping. But the methodology can also be used with data from photogrammetry and LiDAR.

All blocks were identified as keyblocks with the program B02HPGL and afterwards visualised with the program B03HPGL (chapter 5.2.3 and 5.3.3). Thereby the block volume was computed. Next the required friction angle was computed and compared to the available friction angle (chapter 5.2.4 and 5.3.4). In all cases the required friction angle was higher than the available friction angle. Therefore the blocks had failed in nature.

The analysed block moulds could have been identified with block theory. On that account the results of this thesis proof that the application of block theory on natural slopes is not only possible but also allows a rapid identification of hazardous blocks.

7.   APPENDIX

7.1.   BIBLIOGRAPHY

Ahmetovic, E., Kosanovic, A., Yoshida, M.A., Reinisch, J., 2015. Field Methods in Rock Mass Characterization Geo.950.

Buckley, S.J., Howell, J.A., Enge, H.D., Kurz, T.H., 2008. Terrestrial laser scanning in geology: data acquisition, processing and accuracy considerations. J. Geol. Soc. Lond. 165, 625–638.

Campbell, J.B., Wynne, R.H., 2011. Introduction to remote sensing, 5th ed. ed. Guilford Press, New York.

Fekete, S., Diederichs, M., Lato, M., 2010. Geotechnical and operational applicaions for 3-dimensional laser scanning in drill and blast tunnels. Tunneling Undergr. Space Technol. 25.

Goodman, R.E., Hatzor, Y., 1990. Keynote lecture: The influence of geological structure on the engineering of undergorund openings in discontinous rock masses, in: International Association of Engineering Geology (Ed.), Proceedings / Sixth International Congress. Balkema, Rotterdam.

Goodman, R.E., Shi, G., 1985. Block Theory and its Application to Rock Engineering. Englewood Cliffs, Prentice-Hall, London.

Hatzor, Y., 1993. The block failure likelihood: A contribution to rock engineering in blocky rock masses. Int. J. Rock Mech. Min. Sci. Geomech. Abstr. 30, 1591–1597. doi:10.1016/0148-9062(93)90162-7

Hatzor, Y., Goodman, R.E., 1995. Application of block theory and the critical key block concept to tunneling: Two case histories, in: Fractured and Jointed Rock Masses, Myer, Cook, Goodman & Tsang.

Hatzor, Y., Goodman, R.E., 1993. Determination of the design block for tunnel supports in highly jointed rock, in: Comprehensive Rock Engineering.

Kieffer, D.S., 2012. GEO.992 Landslides and slope processes.

Land Steiermark, 2017. Digitaler Atlas Steiermark [WWW Document]. URL www.gis.steiermark.at/cms/ziel/73679/DE/

Liu, Q., 2016. GEO.950 Field Methods in Rock Mass Characteriszation.

Liu, Q., 2014. GEO.840 Rock Mass Characterisation.

Liu, Q., 2004a. B02HPGL.

Liu, Q., 2004b. B03HPGL.

Liu, Q., 2004c. B04HPGL.

Liu, Q., 2004d. B09HPGL.

Liu, Q., Kaufmann, V., 2015. Integrated assessment of cliff rockfall hazards by means of rock structure modelling applied to TLS data: New developments. Presented at the EUROCK.

Liu, Q., Kieffer, D.S., 2012. Digital tunnel mapping using terrestrial LiDAR - a case study. Presented at the EUROCK.

Liu, Q., Kieffer, D.S., 2011. Virtual Outcrop Modeling for 3D Characterization of Engineering Rock Masses. Presented at the ARMA.

Mauldon, M., 1994. Intersection probabilities of impersistent joints. Int. J. Rock Mech. Min. Sci. Geomech. Abstr. 31, 107–115. doi:10.1016/0148-9062(94)92800-2

Molterer, C., 2015. Ingenieurgeologische Methoden zur Erfassung und Beurteilung von Kluftkörpern (Masterarbeit). Technische Universität Graz, Graz.

Riedmüller, G., Schubert, W., 1999. Rock mass modelling in tunneling versus rock mass classification using rating methods, in: Rock Mechanics for Industry. pp. 601–605.

Thiel, K.-H., Wehr, A., 2004. Performance capabilities of laser-scanners-an overview and measurment principle analysis. Int. Arch. Photogramm. Remote Sens. Spat. Inf. Sci. 36, 14–18.

Waltham, T., 2009. Foundations of engineering geology, 3rd ed. ed. Spon Press, London ; New York.

Wietek, B., 2011. Böschungen und Baugruben: ohne und mit Verbau, 1. Aufl. ed, Praxis. Vieweg & Teubner, Wiesbaden.

Wikipedia - Geological compass [WWW Document], 2015. . Wikipedia.org. URL https://upload.wikimedia.org/wikipedia/commons/thumb/1/10/FPM_compass_with_an notation_en.svg/800px-FPM_compass_with_annotation_en.svg.png

7.2. LIST OF FIGURES

7.3. LIST OF TABLES